Received: 13 June 2024 | Revised: 26 July 2024 | Accepted: 19 August 2024

DOI: 10.1002/fft2.473

FOOD FRONTIERS Open Access

RESEARCH ARTICLE

From small-scale studies to an encompassing view: Inhibiting inflammation and clinically relevant enzymes with various extracts of *Primula vulgaris* using in vitro and in silico techniques

Inci Kurt-Celep[1] | **Nilofar**[2,3] | **Mehmet Veysi Cetiz**[4] | **Dimitrina Zheleva-Dimitrova**[5] | **Reneta Gevrenova**[5] | **Engin Celep**[6] | **Kouadio Ibrahime Sinan**[2] | **Evren Yildiztugay**[7] | **Claudio Ferrante**[3] | **Gokhan Zengin**[2]

[1]Faculty of Pharmacy, Department of Biotechnology, Istanbul Okan University, Tuzla, İstanbul, Türkiye

[2]Department of Biology, Science Faculty, Selcuk University, Konya, Turkey

[3]Department of Pharmacy, Botanic Garden "Giardino dei Semplici,", Università degli Studi "Gabriele d'Annunzio,", Chieti, Italy

[4]Department of Bioinformatics, University of Wurzburg, Wurzburg, Germany

[5]Faculty of Pharmacy, Department of Pharmacognosy, Medical University of Sofia, Sofia, Bulgaria

[6]Faculty of Pharmacy, Department of Pharmacognosy, Acibadem Mehmet Ali Aydınlar University, Ataşehir, Istanbul, Türkiye

[7]Science Faculty, Department of Biotechnology, Selcuk University, Konya, Turkey

Correspondence
Gokhan Zengin, Science Faculty, Department of Biology, Selcuk University, 42130 Konya, Turkey.
Email: gokhanzengin@selcuk.edu.tr

Funding information
National Recovery and Resilience Plan of the Republic of Bulgaria, Grant/Award Number: BG-RRP-2.004-0004-C01

Abstract

The genus *Primula* holds great importance as a source of traditional remedies in various folk medicine systems. In the present study, we investigated the chemical composition and biological properties of different extracts (ethyl acetate, ethanol, ethanol/water, and water) of aerial parts and rhizomes of *Primula vulgaris*. To determine the chemical profile, the extracts were analyzed using ultrahigh performance liquid chromatography-high-resolution mass spectrometry (UHPLC-HRMS) technique and flavonoids were a major group in this profile. The antioxidant capacity was demonstrated by in vitro chemical tests and in general the ethanol/water extract was found to be the most potent. Enzyme inhibition was studied against various enzymes and ethanol and ethanol/water extracts were more active than others. To assess the anti-inflammatory potential of the extracts at the molecular level, human dermal fibroblasts (HDF) were treated with lipopolysaccharide (LPS). In vitro experiments showed that the levels of nuclear factor kappa B (NFKB), receptor for advanced glycation end-products (RAGE), activator protein-1 (AP-1), interleukin 6 (IL-6), interleukin 17 (IL-17) and tumor necrosis factor (TNF)-alpha were significantly reduced after treatment with the tested extracts. In addition, the extracts showed an inhibitory effect on the enzymes collagenase, elastase, and hyaluronidase, which are involved in the inflammatory process and destabilization of the extracellular matrix (ECM). *P. vulgaris* has been observed to modulate matrix metalloproteinase (MMP) synthesis by decreasing the concentration of cellular reactive oxygen species (ROS) during LPS-induced inflammation. This study also examined the molecular binding and dynamic behavior of various enzymes and proteins associated with skin and infections using ligands derived from the tested extracts. Simulations with AutoDock Vina V1.1.2 and GROMACS 2023.1 showed that isoquercetin in particular showed superior performance in interactions

with hyaluronidase. These findings are important for the development of potential therapeutic strategies for skin health and infection control. In summary, *P. vulgaris* can be considered as an important source of natural bioactive compounds for the development of effective health-promoting applications in nutraceuticals, pharmaceuticals, and cosmetics

KEYWORDS
anti-inflammatory, antioxidant, flavonoids, in silico assays, *Primula*, skin health

1 | INTRODUCTION

Plants have played a crucial role in providing nourishment and healing to humanity throughout history. Medicinal plants have been widely acknowledged for their therapeutic capabilities and have been highly regarded as an essential asset for human well-being (Ozkan et al., 2017). The existing body of research suggests that phytochemicals found in medicinal plants play a significant role in conferring a diverse range of advantageous characteristics, such as antioxidant, anticancer, antifungal, antiprotozoal, antibacterial and anti-helminthic activities (A. Mohamed et al., 2014; Della Valle et al., 2020; Mohammed et al., 2020; Yerlikaya et al., 2017; Zengin et al., 2018). The antioxidant effects of phytochemicals can help manage important global health problems such as diabetes, Alzheimer's disease and obesity, also known as oxidative stress-related diseases (Jomova et al., 2024). Furthermore, inflammation is a complex biological response involving multiple actors against invading pathogens or harmful stimuli. Therefore, anti-inflammatory agents are becoming increasingly important to manage the complex process. In the last decade, several phytochemicals have been reported as potent anti-inflammatory agents (Gonfa et al., 2023; Yuandani et al., 2024).

Cancer encompasses a diverse group of diseases characterized by the transformation of normal cells into malignant ones, a multifaceted process known as carcinogenesis. Cancer, a major public health concern, continues to be a leading cause of death globally. The number of cases is increasing, especially in Asia, Africa, and the United States as in the United States alone, cancer claims over 570,000 lives annually (Ruddon, 2007; Siegel et al., 2020). Notably, around 70% of cancer-related deaths occur in low- and middle-income countries (Nelson et al., 2020). The treatment regimen for many cancer patients typically includes chemotherapy and radiotherapy. However, these therapies often inadvertently harm healthy cells, and, over time, cancer cells may develop resistance to these treatments, diminishing their effectiveness (Naidu et al., 2004). As a result, there has been an increasing fascination with investigating natural antioxidants and phytochemicals as additional treatments because of their potential to inhibit cell growth and promote cell death (Pucci et al., 2019; Singh et al., 2016). Interestingly, nearly half of all current chemotherapeutic drugs are derived, either directly or indirectly, from compounds found in medicinal plants. This highlights the immense potential of plants as sources for discovering new therapeutic agents (Iqbal et al., 2018). Researchers have been exploring compounds derived from plants in their search for new anticancer agents. In recent years, a significant number of chemical compounds have been authorized for cancer treatment (Agarwal et al., 2020). Various organic molecules, such as terpenes, flavonoids, alkaloids, lignans, saponins, vitamins, glycosides, oils, and other secondary metabolites, play a vital role in selectively inhibiting the growth of cancer cells and promoting cell death (Avtanski & Poretsky, 2018; Iqbal et al., 2018).

The genus *Primula*, the largest within the Primulaceae family, comprises 430 species classified into 7 subgenera and 38 sections. It predominantly thrives in the cold and temperate zones of the Northern Hemisphere (Richards, 2014). *Primula* species include a high concentration of phenolics, terpenes, saponins, tannins, and alkaloids (Mostafa et al., 2014; Ozkan et al., 2017). The members of the genus *Primula* are widely acknowledged for their decorative appeal, and they have also been employed in traditional medicine and utilized as model organisms (Schmidt-Lebuhn et al., 2012). The genus is well regarded in the field of medicine for its effectiveness in mitigating spasms, cramps, rheumatic aches, and paralysis. Saponins found in *Primula* possess expectorant effects. Furthermore, it has been shown that *Primula* flowers possess anodyne, diaphoretic, diuretic, and expectorant components (Jäger et al., 2006). In addition to traditional uses, the flowers of the *Primula* genus are also used as food, especially in the preparation of desserts, salads and beverages (Demasi et al., 2023; Meos et al., 2017; Talreja & Tiwari, 2023; Tarapatskyy et al., 2021). In addition, it has been observed that essential oils derived from *P. vulgaris* exhibit notable antibacterial properties against a range of bacterial species, including *M. smegmatis* (Yaylı et al., 2016). *P. vulgaris*, commonly known as Primrose, is a hairy perennial herb with a stout, short rhizome adorned with old leaf remnants and numerous fleshy roots (Jacquemyn et al., 2009). Many species of *Primula* including *P. vulgaris* frequently used in traditional medicine (Colombo et al., 2017). They are recognized for their high saponin content (Coran & Mulas, 2012). They are also listed in the European Pharmacopoeia (Länger, 2012).

The aim of this study was to evaluate the phytochemical composition of different extracts obtained from *P. vulgaris* aerial parts and rhizomes using UHPLC-HRMS analysis. Furthermore, the study planned to examine their potential in vitro antioxidative, anti-diabetic, anti-Alzheimer, and anti-inflammatory activities. Healthy human dermal fibroblast (HDF) cells were used as a control cell group, while lipopolysaccharide (LPS) was used as a trigger for the inflammation

TABLE 1 Extraction yields (%), total phenolic and flavonoid contents in the *Primula vulgaris* extracts.

Parts	Solvent	Extraction yields (%)	TPC (mg GAE/g)	TFC (mg RE/g)
Aerial parts	EA	2.26	29.27 ± 0.16^{cd}	3.30 ± 0.32^{d}
	Ethanol	5.00	32.07 ± 0.76^{b}	7.68 ± 0.43^{c}
	Ethanol/water	19.28	29.67 ± 0.49^{c}	47.94 ± 0.18^{a}
	Water	9.94	27.96 ± 0.39^{de}	26.48 ± 0.47^{b}
Rhizomes	EA	0.94	30.48 ± 0.53^{c}	2.62 ± 0.14^{d}
	Ethanol	7.7	27.48 ± 0.07^{e}	1.44 ± 0.03^{e}
	Ethanol/water	21.20	40.98 ± 0.94^{a}	1.64 ± 0.08^{e}
	Water	12.64	29.26 ± 0.50^{cd}	1.64 ± 0.08^{e}

TPC: total phenolic content; TFC: total flavonoid content. GAE: gallic acid equivalent; RE: rutin equivalent.
Note: Values are reported as mean ± SD of three parallel experiments. Different letters$^{(a-e)}$ indicate significant differences between the tested extracts ("a" indicate the highest content, $p < .05$).

pathway in these cells. For the treatment of inflammation caused by inducing HDF cells with LPS, different extracts obtained from the rhizome and air part of *P. vulgaris* at nontoxic concentrations were applied to these cells (HDF+LPS). The levels of phospho-NFKB, RAGE, AP-1, IL-6, IL-17, and TNF-alpha proteins, which are active in the inflammation pathway, were examined. Additionally, it was observed that *P. vulgaris* applied to the HDF+LPS cell group reduced the ovarian expression of collagenase, elastase, and hyaluronidase enzyme activities, which cause delays in the formation of the skin barrier in chronic skin injuries, to basal levels. On the other hand, the activation of MMP-2 and MMP-9, which play a role in the remodeling of the extracellular matrix, was investigated.

2 | MATERIALS AND METHODS

2.1 | Plant collection

Plant materials were gathered in 2023 from Konya: Kestel Forest, 1400 m. Taxonomic identification, performed by Dr. Evren Yildiztugay and a voucher specimen was deposited in the herbarium of Selcuk University (Voucher number: EY-2992). Aerial parts and rhizomes were meticulously separated, dried in the shade at room temperature, ground and stored in darkness.

2.2 | Plant extract preparation

Four solvents; ethyl acetate, ethanol, ethanol/water (70%) and water were utilized in the preparation of extracts. About 10 g of the sample were macerated with 200 mL of ethyl acetate, ethanol, and ethanol/water for 24 h at room temperature. The water extract was obtained by soaking 10 g of plant material in boiled water for 15 min using the infusion method. The organic solvents were then evaporated under reduced pressure, and the water extract was lyophilized using a freeze dryer. Extraction yields (%) are given in Table 1.

2.3 | Assay for total phenolic and flavonoid contents

According to the methods specified by (Slinkard & Singleton, 1977), total phenolics and flavonoids were quantified. Gallic acid (GA) and rutin (RE) served as standards in the assays, and the outcomes were reported as gallic acid equivalents (GAE) and rutin equivalents.

2.4 | UHPLC-HRMS dereplication/annotation

The UHPLC-HRMS analyses were performed as previously described (Zheleva-Dimitrova et al., 2023) on a Q Exactive Plus mass spectrometer (ThermoFisher Scientific, Inc.) equipped with a heated electrospray ionization (HESI-II) probe (ThermoScientific). The equipment was operated in negative and positive ion modes within the *m/z* range from 130 to 2000. The chromatographic separation was achieved on a reversed phase column Kromasil EternityXT C18 (1.8 µm, 2.1 × 100 mm) at 40°C. The UHPLC analyses were run with a mobile phase contained 0.1% formic acid in water (A) and 0.1% formic acid in acetonitrile (B). The run time was 33 min. The flow rate was 0.3 mL/min. The gradient elution program was used as follows: 0–1 min, 0–5% B; 1–20 min, 5–30% B; 20–25 min, 30–50% B; 25–30 min, 50–70% B; 30–33 min, 70–95%; 33–34 min 95–5%B. Equilibration time was 4 min. The injection volume and the flow rate were set to 1 µL and 300 µL/min, respectively. Data acquisition was performed using Xcalibur 4.2 (ThermoScientific, Waltham, MA, USA) instrument control/data handling software.

2.5 | Assays for in vitro antioxidant capacity

According to the methods provided by Grochowski et al. (2017), antioxidant tests were executed. The DPPH, ABTS radical scavenging, CUPRAC, and FRAP test results were expressed as milligrams of Trolox equivalents (TE) per gram of extract. The antioxidant potential

determined by the phosphomolybdenum (PBD) assay was measured in millimoles of Trolox equivalents (TE) per gram of extract, and metal chelating activity (MCA) was conveyed as milligrams of disodium edetate equivalents (EDTAE) per gram of extract.

2.6 | Inhibitory effects against some key enzymes

Enzyme inhibition experiments on the samples were conducted following established protocols (Grochowski et al., 2017). Amylase and glucosidase inhibition were quantified in acarbose equivalents (ACAE) per gram of extract, while acetylcholinesterase (AChE) and butyrylcholinesterase (BChE) inhibition were expressed in milligrams of galanthamine equivalents (GALAE) per gram of extract. Tyrosinase inhibition was measured in milligrams of kojic acid equivalents (KAE) per gram of extract.

2.7 | Molecular docking

Proteins and enzymes were obtained from the Protein Data Bank. Co-crystallized ligands, cofactors, and waters were extracted using BIOVIA Discovery Studio Visualizer V4.5. Ligands were obtained from PubChem and optimized with OpenBabel V3.1.1. Structure preparation included addition of polar hydrogens and energy minimization using MGL Tools V1.5.6. Active sites were identified through CASTp V3.0, POCASA V1.0 and literature (Huang et al., 2023). Molecular docking was performed using AutoDock Vina V1.1.2 with specified grid boxes (Trott & Olson, 2010).

2.8 | Molecular dynamic simulation

Molecular dynamics (MD) simulations were set up via the CHARMM GUI platform (https://charmm-gui.org/) (Jo et al., 2008), employing the Solution Builder for system setup. Proteins were parameterized using the CHARMM36m force field (Arabi-Jeshvaghani et al., 2023; Maier et al., 2015). A periodic boundary box was filled with TIP3P water, ensuring a minimum 10 Å buffer between the protein and box edges. System neutralization was achieved by adding counterions to reach a 0.15 M NaCl concentration. Electrostatic and van der Waals interactions were managed using the Verlet cutoff scheme, while the LINCS algorithm secured bond lengths. Long-range electrostatics were computed using the particle mesh Ewald (PME) method. The system was initially relaxed via steepest descent energy minimization, maintaining potential energy changes below 1000 kj/mol/nm. Subsequent equilibrium stages included a constant volume and temperature (NVT) phase at 300 K and a constant pressure and temperature (NPT) phase, utilizing a thermostat and barostat, respectively. These steps ensured thermodynamic stability and proper energy and particle exchange. The simulation extended over 100 ns (nstep = 50000000) using GROMACS 2023.1 (Maier et al., 2015) at a steady 310.05 K. Postsimulation, trajectory analyses via gmx_energy, gmx_rms, gmx_rmsf, and gmx_gyrate modules assessed various metrics like total energy, RMSD, RMSF, number of hydrogen bonds, solvent accessibility, and gyration radius.

2.9 | Inhibition of advanced glycation end products (AGEs)

In order to demonstrate the inhibitory potential of eight extracts obtained from different parts of the *P. vulgaris* on the formation of advanced glycation end products (AGEs), the protocol we have previously optimized was followed (Kurt-Celep et al., 2023; Kurt-Celep et al., 2022). In this context, eight different *P. vulgaris* plant extracts in 1 and 10 mg/mL bovine serum albumin (BSA) and 0.5 M glucose were mixed in equal volumes and incubated at 55°C for 40 h. The group that did not include the plant sample was used as a control group and quercetin in increasing concentrations (62.5–1000 µg/mL) was selected as a positive control (Kurt-Celep et al., 2023; Kurt-Celep et al., 2022). Following the end of the incubation period, the fluorescence intensity in the samples was measured in the 370 nm excitation/440 nm emission range on a Thermo Scientific™ Varioskan™ LUX multimode microplate reader.

2.10 | Cell culture and viability

HDF has been selected as the cell line in which the skin damage triggered by the inflammation pathway by LPS was mimicked in vitro conditions. HDF cells commercially sourced from ATCC were cultivated in a mammalian cell culture of 5% CO_2 at 37°C in Dulbecco's Modified Eagle Medium (DMEM), which contains 10% fetal bovine serum and 1% penicillin/streptomycin. Untreated HDF cells were used as a control group, while 10 µg/mL of LPS-treated HDF cells were used as the sample group (Mosxou & Letsiou, 2021; Shi et al., 2021). The WST-1 test was used to determine the nontoxic concentration of the tested extracts, which were used to treat HDF cells whose inflammation pathway was induced by LPS (Kurt-Celep et al., 2024). In this context, HDF control cells and HDF+LPS cells in the experimental setup were planted in a 96-well plate at a density of 10,000/well, and at the end of the 16th hour, the tested extracts in increasing concentrations were applied to the HDF+LPS cells for 48 h. After 48 h, to test the viability of the cells due to toxicity, 1:10 diluted WST-1 dye was applied to the cells for 1 h and the colorimetric change was measured with the help of a microplate reader at 570 nm (Barak et al., 2023; Kurt-Celep et al., 2024).

2.11 | Determination of mitochondrial antioxidant level with DCFDA

The amount of ROS increased in the cells as a result of inflammation stimulated by LPS-induced HDFS, the amount of ROS scavenged after the application of *P. vulgaris* extracts was determined using the DCFDA method. The ROS scavenging potential of *P. vulgaris* was determined

using the method previously described in the literature (Barak et al., 2023; Kurt-Celep et al., 2024). In the experimental setup, untreated-HDF cells were used as the control group, while the epigallocatechin gallate (EGCG) standard was selected as a positive control (Barak et al., 2023; Kurt-Celep et al., 2024).

2.12 | Western blot

After applying the tested extracts to HDF cells whose inflammation mechanism was activated by LPS, varying levels of phospho-NFKB, RAGE, AP-1, IL-6, IL-17, and TNF-alpha proteins were detected by the Western blot technique, respectively. One of the universal loading controls, the housekeeping protein beta-actin, has been used as proof of equal protein loading (Kurt-Celep et al., 2023; Kurt-Celep et al., 2024; Kurt-Celep et al., 2021). On the other hand, a 20% gel composition for separating gel and a 4% stacking-gel composition were prepared for the distinctive gel due to the molecular weight of the target proteins to be controlled in the Western blot. Then, proteins at a concentration of 30 µg/µL obtained from whole-cell lysate were loaded into all wells. To clearly separate the proteins in the separating gel, they were electrophoresed in the cold running buffer for approximately 4 h. After, the membrane was treated with the relevant antibodies, and the band was imaged with the Chemicdoc device (Kurt-Celep et al., 2022).

2.13 | Activity or inhibition of enzymes linked between extracellular matrix (ECM) regulation

The inhibitory activity of *P. vulgaris* extracts at a concentration of 1 mg/mL on the enzyme's collagenase, elastase, and hyaluronidase respectively was carried out following the optimized protocol previously presented in the literature (Barak et al., 2023; Barak et al., 2022; Ersoy et al., 2019). In the anti-collagenase and anti-elastase tests, EGCG was selected as the positive control, while tannic acid was used in the anti-hyaluronidase test. At the end of the 80th minute, inhibition activity was determined by taking measurements with the help of a microplate reader.

2.14 | Jelatinaz Zimografi for MMP-2 and MMP-9

The biosynthesis of matrix metalloproteinases involved in the formation of ECM partners in dermal fibroblast cells in which the inflammation pathway was induced by LPS was determined by the gelatine zymography method (Kurt-Celep et al., 2023; Kurt-Celep et al., 2024). In this context, the extracts obtained from *P. vulgaris* were applied to LPS-treated HDF cells for 48 h, and the cells' media were collected to obtain MMPs released into the extracellular matrix. Then, equal volumes of media were mixed with SDS-free 1× loading dye and loaded onto the PAGE gel containing gelatine (Barak et al., 2023; Kurt-Celep et al., 2023; Kurt-Celep et al., 2024). The gel was run in a cold tank to avoid affecting the enzyme activity and to avoid false positive results. If MMPs were active, they broke down the gelatin substrates in the gel and gave white lytic band images (Kurt-Celep et al., 2022; Kurt-Celep et al., 2022). Gels were painted with Coomassie blue brilliant dye to make the white lithic fields in the wells visible and imaged with the Bio-Rad Chemidoc device (Barak et al., 2023; Kurt-Celep et al., 2023; Kurt-Celep et al., 2022; Kurt-Celep et al., 2024; Kurt-Celep et al., 2022; Kurt-Celep et al., 2023).

2.15 | Data analysis

Clustered Image Maps (CIMs) were generated to visualize the variation in biomolecules across the samples. Subsequently, dataset of the biological activities underwent principal component analysis (PCA) and Clustered Image Map (CIMs) analysis, respectively. For CIMs analysis, we used the Euclidean distance classifier and Ward's clustering method. Prior to the PCA and CIMs analysis, the data underwent centering and normalization. Lastly, Pearson's correlation coefficients were computed to examine the associations between biomolecules and antioxidant as well as enzyme inhibitory activities. In addition, the ordinary one-way ANOVA tab of the GraphPad analysis program was used in the statistical analysis of AGEs, detection of mitochondrial ROS level by DCFDA, collagenase, elastase, hyaluronidase enzyme inhibition assays and zymography experiments. On the other hand, the two-way ANOVA Multiple comparison tab of GraphPad analysis program was used for statistical analysis of WST-1 and Western blot experiments. In all experiments, the statistical value with the smallest significance was accepted as $p \leq .05$ and symbolized by *.

3 | RESULTS AND DISCUSSION

3.1 | Total phenolic and flavonoid contents

In a study examining the total phenolic content (TPC) and total flavonoid content (TFC) of *P. vulgaris* extracts, derived from both its aerial parts and rhizomes using various solvents, significant variations were observed across the different extractions. For the aerial parts, the highest TPC was noted in extracts obtained with ethanol, showing a value of 32.07 mg GAE/g, while the lowest was found in those extracted with water, recording a TPC of 27.96 mg GAE/g. Conversely, the ethanol/water mixture yielded the most remarkable result in terms of TFC, with a strikingly high value of 47.94 mg RE/g, compared to the lowest TFC observed in the EA extracts, which was 3.30 mg RE/g. In the case of the rhizomes, the extracts exhibited a different trend. The ethanol/water presented the highest value of TPC 40.98 mg GAE/g. The lowest TPC among the rhizome extracts was found with ethanol, showing a value of 27.48 mg GAE/g. Regarding TFC, the lowest content was similarly observed in the ethanol extracts, which had a minimal value of 1.44 mg RE/g. Both the water and the ethanol/water extracts of the rhizomes displayed similar TFC values of 1.64 mg RE/g, which were among the lowest values reported in the study (Table 1).

These findings highlight the impact of solvent choice on the extraction efficiency of phenolic and flavonoid compounds from *P. vulgaris*, with ethanol and ethanol/water mixtures showing effectiveness for

extracting phenolic compounds from the aerial parts and rhizomes, respectively. The ethanol/water mixture significantly enhanced the flavonoid extraction from the aerial parts, suggesting a solvent-specific affinity for different types of phytochemicals within the plant. In a study, a contrasting perspective was presented through UPLC–PDA–MS/MS analysis of the root extracts of *P. veris*, revealing that, among the various morphological parts examined, the roots contained relatively low levels of polyphenolic compounds (Tarapatskyy et al., 2021). This observation is consistent with existing scientific literature (Coran & Mulas, 2012), which suggests that the underground parts of *Primula*, notable for their high saponin content, are commonly utilized in pharmaceutical formulations for their expectorant properties. This has led to an expectation that their polyphenolic activity would be minimal compared to other parts of the plant. In agreement with our results, previous study demonstrated that ethanolic extracts from the roots of *P. veris* actually possess a significant phenolic content, with concentrations ranging between 131 to 168 mg GAE/L for roots and 136 to 159 mg GAE/L for leaves (Lupitu et al., 2018). This suggests that a more detailed understanding of the plant's biochemical profile is necessary.

3.2 | UHPLC-HRMS dereplication/annotation

Based on the comparison with reference standards and literature data of the retention times, MS and MS/MS accurate masses, fragmentation patterns in MS/MS spectra, and relative ion abundance, a total of 74 secondary metabolites were identified or tentatively annotated in *Primula vulgaris* extracts (Table 2).

3.2.1 | Hydroxybenzoic, hydroxycinnamic acids, alcohols, and derivatives

Hydroxybenzoic acids (7, 11, 14, 15, 23, and 33), their glycosides (1–6, 8–10, 16, 19, 20, and 22), hydroxycinnamic acids (13, 18, 21, and 29), their glycosides (12, 17, 24) were identified based on comparison with reference standards and literature data (Table 1) (Gevrenova et al., 2020). Compounds 31 and 32 $[M-H]^-$ at *m/z* 475.146 gave a base peak at *m/z* 293.088 $[C_{11}H_{17}O_9]^-$, corresponding to the loss of methyl-hydroxy-methoxybenzoyl residue from the primverosyl moiety. The subsequent loss of glucosyl residue at *m/z* 131.036 was indicative for the structure of primulaverin/primverin, previously found in *Primula* species (Table 1) (Figure S1). Similarly, primverosides of guaiacol (25), 4-hydroxy-3-methoxy-benzoyl alcohol (26 and 27), as well as gaultherin (30) were annotated in the studied extracts (Stefanis et al., 2023).

3.2.2 | Flavonoids

In general, 1 flavanol, 19 flavones, and 21-flavonols and their glycosides were assigned in the studied *P. vulgaris* extracts. The flavonoid annotation/dereplication was based on the diagnostic ions and their relative abundances. Detailed discussion on the MS/MS fragmentation patterns of different subclasses flavonoids was previously described (Gevrenova et al., 2020; Gevrenova et al., 2022). Compound 34 ($[M-H]^-$ at *m/z* 305.067) was tentatively annotated as gallocatechin/epigallocatecin based on the fragments at *m/z* 261.077 ($[M-H-CO_2]^-$), 243.067 ($[M-H-CO_2-H_2O]^-$), 233.082 ($[M-H-CO_2-CO]^-$), as well as Retro-Diels-Alder (RDA) reaction ions at *m/z* 125.023 ($^{1,4}A^-$) and 109.028 ($^{0,4}A^-$). Key step in the dereplication/annotation of flavonoid glycosides was the neutral loss of 162.05, 146.05, 132.04, 324.1, 486.15, and 308.1 Da, corresponding to hexose, deoxyhexose, pentose, dihexose, trihexose, and rutinose (Zengin et al., 2019). Depending on the intensity and the ratio of the fragment ions $[Y0]^-$ and $[Y0-H]^-$, the sites for binding the sugar parts to the aglycones were also determined (Pascale et al., 2020).

The flavones in the studied species were *O*-glycosides of apigenin ($[Agl-H]^-$ at *m/z* 283.061) (58), luteolin ($[Agl-H]^-$ at *m/z* 285.041) (52 and 57), nepetin ($[Agl-H]^-$ at *m/z* 315.049) (44, 49), 4′,7-dihydroxy-3′-methoxyflavone ($[Agl-H]^-$ at *m/z* 283.061) (41, 62), 4′-hydroxyflavone ($[Agl-H]^-$ at *m/z* 253.051 (59, 60), flavone ($[Agl-H]^-$ at *m/z* 237.055) (61, 64). The flavone aglycons 3′,4′,5′-trihydroxyflavone (63) luteolin (65), 3′,4′-dihydroxyflavone (67), 4′,7-dihydroxy-3′-methoxyflavone (68), apigenin (69), chrysoeriol (71), 4′-hydroxyflavone (73), 7-*O*-methylluteolin (74) were also identified in the studied *Primula* extracts (Table 2). Compound 41 ($[M-H]^-$ at *m/z* 607.167) gave a base peak at *m/z* 283.061 $[M-H-2hex]^-$, together with fragment ions at *m/z* 268.038 $[Agl-CH_3^{\bullet}]^-$, 239.035 $[Agl-CH_3^{\bullet}-CHO]^-$, and 211.040 $[Agl-CH_3^{\bullet}-CHO-CO]^-$. Based on the RDA fragments at *m/z* 148.016 ($^{0,4}B^-$) and 119.013 ($^{0,3}A^-$), 41 was tentatively annotated as 4′-hydroxy-3′-methoxyflavone-7-*O*-dihexoside (Figure S2) (Table 2). In addition, glycosides of the flavonols quercetin (35, 38, 39, 45, 48, 55), kaempferol (40, 43, 47, and 54), isorhamnetin (36, 37, 42, 46, 50, 51, 53, and 56), as well as flavonol aglycones quercetin (66), kaempferol (70), isorhamnetin (72) were dereplicated in the *P. veris* extracts (Table 2). Compounds 43, 45, 48, 52, 53, 54, 55, 56, 57, 58, 65, 66, 69, 70, 71, and 72 were identified based on comparison with reference standards. Structures of identified/tentatively annotated flavonoids were presented in Figure S3.

3.3 | Antioxidant activity

Antioxidants are substances that can neutralize harmful chemicals called free radicals, which can cause damage to cells and DNA. Oxidative damage is a causal element in the development of cancer. Therefore, antioxidants play a crucial role in the prevention of cancer by reducing oxidative stress and cellular damage (Kocyigit et al., 2018). Table 3 presented diverse antioxidant capacities as measured by DPPH, ABTS, CUPRAC, FRAP, PBD, and MCA assays. For the aerial parts, the ethanol/water extract demonstrated the highest antioxidant activity in the DPPH assay, achieving a value of 39.89 mg TE/g, which was significantly greater than the lowest recorded value of 4.65 mg TE/g for the EA extract. This high antioxidant activity correlates with the previously noted high TFC value for the ethanol/water extract,

TABLE 2 Specialized metabolites in *Primula vulgaris* in (−) ESI-MS/MS.

No	Identified/tentatively annotated compound	Molecular formula	Exact mass [M-H]⁻	Fragmentation pattern in (-) ESI-MS/MS	t_R (min)	Δ ppm	Distribution
Hydroxybenzoic, hydroxycinnamic acids and alcohols and derivatives							
1.	Protocatechuic acid-*O*-hexoside isomer I	$C_{13}H_{16}O_9$	315.0722	315.0732 (0.3), 153.0182 (100), 135.0441 (1.7, 125.0223 (0.2), 109.0281 (20.2)	1.09	3.443	4, 5, 6, 7, 8
2.	Hydroxybenzoic acid-*O*-hexoside isomer I	$C_{13}H_{16}O_8$	299.0772	299.0762 (0.2), 137.0231 (100), 93.0330 (66.0)	1.27	−3.580	1, 2, 4, 5, 6, 7, 8
3.	Protocatechuic acid-*O*-hexoside isomer II	$C_{13}H_{16}O_9$	315.0722	315.0728 (100), 153.0182 (59.6), 135.0075 (25.3), 109.0281 (73.8)	1.44	2.078	2, 3, 4, 5, 6, 7, 8
4.	Galloyl-*O*-hexoside	$C_{13}H_{16}O_{10}$	331.0671	331.0675 (10.1), 169.0133 (100), 125.0231 (45.1)	1.57	1.420	2, 3, 4, 5, 6, 7, 8
5.	Protocatechuic acid-*O*-hexoside isomer III	$C_{13}H_{16}O_9$	315.0722	315.0729 (20.9), 153.0182 (100), 135.0440 (0.2), 109.0281 (54.9)	1.74	2.491	2, 3, 5, 6, 7, 8
6.	Vanillic aid-*O*-hexoside isomer I	$C_{14}H_{18}O_9$	329.0878	329.0887 (1.8), 209.0446 (0.2), 167.0339 (100), 152.0103 (21.9), 123.0438 (14.4), 108.0202 (35.9)	1.74	2.658	2, 3, 4, 5, 6, 7, 8
7.	Protocatechuic acid[a]	$C_7H_6O_4$	153.0193	153.0182 (17.87), 109.0280 (100)	2.02	−7.201	1, 2, 3, 4, 5, 6, 7, 8
8.	Hydroxybenzoic acid-*O*-hexoside isomer II	$C_{13}H_{16}O_8$	299.0772	299.0778 (100), 239.0559 (20.9), 209.0456 (5.9), 179.0342 (46.9), 137.0232 (87.3), 93.0331 (18.9)	2.03	1.837	2, 3, 4, 5, 6, 7, 8
9.	*p*-Hydroxyphenylace acid-*O*-hexoside isomer I	$C_{14}H_{18}O_8$	313.0929	313.0934 (0.2), 151.0389 (100), 109.0281 (5.9), 107.0487 (3.7)	2.17	1.563	3, 4, 5, 7, 8
10.	Syringic acid-*O*-hexoside	$C_{15}H_{20}O_{10}$	359.0984	359.0989 (8.7), 197.0448 (100), 182.0212 (19.7), 166.9975 (7.8), 153.0547 (14.8), 138.0310 (27.3), 123.0074 (31.2)	2.25	1.504	2, 3, 4, 5, 6, 7, 8
11.	Syringic acid[a]	$C_9H_{10}O_5$	197.0455	197.0448 (30.3), 182.0211 (100), 166.9975 (57.6), 139.0023 (29.5), 123.0074 (36.4)	2.26	−3.891	5, 6, 7, 8
12.	Caffeic acid-*O*-hexoside isomer I	$C_{15}H_{18}O_9$	341.0878	341.0878 (3.8), 179.0341 (100), 161.0596 (0.9), 135.0439 (55.4), 107.0483 (0.3)	2.39	−0.016	2, 3, 4, 5, 7, 8
13.	*p*-Coumaric acid[a]	$C_9H_8O_3$	163.0401	163.0390 (9.6), 135.0439 (4.1), 119.0488 (100)	2.46	−6.363	2, 3, 4, 5, 6, 7, 8
14.	4-Hydroxybenzoic acid	$C_7H_6O_3$	137.0244	137.0232 (100), 119.0126 (2.3), 108.0202 (8.9), 93.0332 (3.8)	2.83	−9.030	2, 3, 4, 5, 6, 7, 8
15.	Gentisic acid[a]	$C_7H_6O_4$	153.0193	153.0183 (52.7), 123.0074 (27.3), 108.0202 (100)	2.97	−7.005	1, 4, 5, 6, 7, 8
16.	*p*-Hydroxyphenylacetic acid-*O*-hexoside isomer II	$C_{14}H_{18}O_8$	313.0929	313.0935 (12.8), 151.0388 (100), 123.0074 (0.7), 109.0281 (3.4)	2.98	1.882	2, 5, 6, 7
17.	Caffeic acid-*O*-hexoside isomer II	$C_{15}H_{18}O_9$	341.0878	341.0883 (29.5), 179.0340 (100), 135.0438 (66.4), 107.0486 (0.7)	3.05	1.509	1, 3, 4, 5, 6, 7, 8
18.	Chlorogenic acid	$C_{16}H_{18}O_9$	353.0878	353.0879 (31.9), 191.0554 (100), 161.0232 (1.9), 93.0331 (3.1)	3.19	0.240	6, 7, 8

(Continues)

TABLE 2 (Continued)

No	Identified/tentatively annotated compound	Molecular formula	Exact mass [M-H]$^-$	Fragmentation pattern in (-) ESI-MS/MS	t_R (min)	Δ ppm	Distribution
19.	Sinapic acid-*O*-hexoside	$C_{17}H_{22}O_{10}$	385.1140	431.1207 (6.2) ([M-H]$^-$+CH_2O_2), 385.1150 (26.6), 223.0608 (100), 208.0373 (8.3), 193.0135 (5.2), 179.0706 (15.2), 164.0469 (24.1), 149.0233 39.0), 137.0231 (37.6)	3.30	2.519	2, 3, 4, 5, 6, 7, 8
20.	Vanillic aid-*O*-hexoside isomer II	$C_{14}H_{18}O_9$	329.0878	329.0886 (4.9), 167.0339 (100), 152.0103 (21.2), 123.0438 (7.1), 108.0202 (57.6)	3.50	2.293	1, 2, 3, 4, 5, 6, 7, 8
21.	Caffeic acid	$C_9H_8O_4$	179.0350	179.0341 (20.7), 135.0439 (100), 107.0488 (1.1)	3.53	−4.759	3, 4, 5, 6, 7, 8
22.	Vanilic acid-*O*-primeveroside	$C_{19}H_{26}O_{13}$	461.1301	461.1311 (42.8), 167.0339 (100), 152.0103 (23.5), 135.0075 (3.0), 108.0202 (36.4), 89.0229 (4.3), 71.0123 (5.9)	4.33	2.312	2, 3, 4, 5, 6, 7, 8
23.	3-Hydroxybenzoic acid	$C_7H_6O_3$	137.0244	137.0234 (9.1), 93.0331 (100)	3.70	−7.352	1, 2, 3, 4, 5, 6, 7, 8
24.	Caffeic acid-*O*-hexoside isomer III	$C_{15}H_{18}O_9$	341.0878	341.0868 (16.2), 179.0704 (100), 135.0439 (45.5)	3.78	−2.977	5, 6, 8
25.	Guaiacol-*O*-primeveroside	$C_{18}H_{26}O_{11}$	417.1402	463.1480 (10.2) ([M-H]$^-$+CH_2O_2), 417.1410 (24.6), 293.0884 (100), 233.0664 (4.5), 191.0556 (4.4), 131.0338 (8.4), 123.0438 (9.8), 108.0202 (15.3)	3.83	5.022	3, 4, 5, 6, 7, 8
26.	4-Hydroxy-3-methoxy-benzoyl alcohol-*O*-primeveroside isomer I	$C_{19}H_{28}O_{12}$	447.1508	493.1579 (15.0) ([M-H]$^-$+CH_2O_2), 447.1516 (35.7), 293.0883 (100), 233.0672 (3.6), 191.0554 (5.2), 161.0449 (0.7), 153.0544 (4.0), 149.0444 (10.8), 138.0311 (9.9), 131.0337 (11.8), 89.0229 (39.4), 71.0123 (38.0)	3.96	3.288	4, 5, 6, 7, 8
27.	4-Hydroxy-3-methoxy-benzoyl alcohol-*O*-primeveroside isomer II	$C_{19}H_{28}O_{12}$	447.1508	493.1578 (9.4) ([M-H]$^-$+CH_2O_2), 447.1517 (20.0), 293.0883 (100), 233.0660 (3.6), 191.0556 (3.8), 161.0441 (0.6), 153.0545 (9.1), 149.0444 (10.5), 131.0338 (7.8), 89.0229 (34.4), 71.0123 (35.0)	4.09	1.947	4, 5, 6, 7, 8
28.	Roseoside	$C_{19}H_{30}O_8$	385.1868	431.1932 (81.2) ([M-H]$^-$+CH_2O_2), 385.1875 (100), 223.1335 (13.0), 205.1227 (9.3), 161.0448 (11.3), 153.0911 (21.7)	4.15	2.249	1, 2, 3, 4, 5, 6, 7, 8
29.	*o*-Coumaric acid[a]	$C_9H_8O_3$	163.0401	163.0390 (9.2), 119.0489 (100)	4.56	−6.240	2, 3, 4, 5, 6, 7, 8
30.	Gaultherin	$C_{19}H_{26}O_{12}$	445.1352	491.1420 (7.7) ([M-H]$^-$+CH_2O_2), 445.1364 (3.1), 293.0883 (100), 233.0670 (2.8), 191.0548 (4.0), 151.0389 (35.0), 137.0230 (3.9), 131.0337 (8.5)	4.38	2.792	1, 2, 3, 4, 5, 6, 7, 8
31.	Primulaverin/primverin	$C_{20}H_{28}O_{13}$	475.1457	521.1531 (9.5) ([M-H]$^-$+CH_2O_2), 475.1480 (5.2), 443.1202 (9.6), 293.0883 (100), 233.0666 (2.6), 191.0555 (4.2), 181.0499 (11.1), 166.0262 (20.5), 149.0444 (11.2), 131.036 (6.8),	4.69	3.738	1, 2, 3, 4, 5, 6, 7, 8

(Continues)

TABLE 2 (Continued)

No	Identified/tentatively annotated compound	Molecular formula	Exact mass [M-H]$^-$	Fragmentation pattern in (-) ESI-MS/MS	t_R (min)	Δ ppm	Distribution
32.	Primulaverin/primverin	$C_{20}H_{28}O_{13}$	475.1457	521.1526 (7.3) ([M-H]$^-$+CH_2O_2), 475.1443 (2.5), 443.1195 (0.5), 293.0883 (100), 233.0670 (2.6), 191.0549 (4.0), 181.0498 (29.4), 166.0263 (0.9), 149.0443 (11.1), 131.036 (6.6)	5.04	−3.060	1, 2, 3, 4, 5, 6, 7, 8
33.	Salicylic acid	$C_7H_6O_3$	137.0244	137.0231 (11.2), 93.0331 (100), 65.0380 (0.8)	6.26	−9.614	1, 2, 3, 4, 5, 6, 7, 8
Flavonoids							
34.	Gallocatechin/epi	$C_{15}H_{14}O_7$	305.0667	305.0673 (100), 287.0567 (0.5), 261.0773 (9.0), 243.0665 (2.1), 219.0660 (18.4), 191.0710 (0.3), 179.0341 (27.7), 137.0231 (30.8), 125.0230 (96.2), 109.0281 (15.2)	2.80	1.914	5, 6, 7, 8
35.	Quercetin 3,7-*O*-dihexoside	$C_{27}H_{30}O_{17}$	625.1410	625.1429 (100), 463.0891 (18.6), 462.0815 (34.6), 301.0359 (31.6), 300.0262 (6.6), 299.0202 (37.9), 271.0251 (41.0), 178.9977 (1.6), 151.0023 (4.6), 107.0126 (1.7)	3.40	2.971	2, 3, 4
36.	Isorhamnetin 3-*O*-dihexoside-7-*O*-hexoside	$C_{34}H_{42}O_{22}$	801.2095	801.2106 (22.2), 639.1586 (100), 315.0516 (98.3), 314.0433 (11.7), 300.0271 (19.1), 271.0245 (14.7), 227.0349 (1.8), 151.0024 (5.1)	3.71	1.341	2, 3, 4
37.	Isorhamnetin 3,7-*O*-dihexoside	$C_{28}H_{32}O_{17}$	639.1567	639.1585 (100), 477.1044 (28.8), 315.0516 (49.9), 314.0435 (9.6), 300.0278 (9.1), 151.0022 (3.0), 107.0125 (0.7)	3.98	2.875	3, 4
38.	Quercetin *O*-trihexoside	$C_{33}H_{40}O_{22}$	787.1939	787.1965 (100), 625.1440 (0.3), 301.0356 (97.5), 300.0280 (80.2), 271.0251 (54.1), 255.0300 (26.7), 178.9978 (9.5), 151.0026 (23.2), 121.0282 (3.7), 107.0124 (9.2)	4.24	3.334	1, 2, 3, 4, 6, 7, 8
39.	Quercetin 3-*O*-dihexoside	$C_{27}H_{30}O_{17}$	625.1410	625.1426 (100), 301.0353 (43.9), 300.0278 (66.4), 271.0251 (35.4), 255.0299 (16.6), 227.0347 (2.7), 178.9979 (3.6), 151.0026 (7.9), 107.0124 (3.1)	4.55	2.587	2, 4
40.	Kaempferol 3-*O*-trihexoside	$C_{33}H_{40}O_{21}$	771.1989	771.2010 (51.3), 285.0407 (100), 255.0301 (19.4), 227.0347 (13.9), 151.0028 (2.4), 135.0076 (1.6)	4.73	2.670	1, 2, 3, 4, 5, 6, 7,8
41.	4′-Hydroxy-3′-methoxyflavone 7-O-dihexoside	$C_{28}H_{32}O_{15}$	607.1668	607.1687 (63.2), 283.0614 (100), 268.0380 (50.8), 239.0349 (28.2), 211.0396 (2.6), 148.0155 (1.1), 119.0125 (0.4)	4.79	3.058	2, 3, 4
42.	Isorhamnetin 3-*O*-trihexoside	$C_{34}H_{42}O_{22}$	801.2095	801.2119 (68.8), 315.0516 (100), 301.0313 (2.0), 300.0279 (26.2), 271.0251 (35.4), 255.0300 (18.5), 227.0344 (3.8), 151.0024 (2.8), 107.0127 (1.1)	4.85	2.938	1, 2, 3, 4, 6, 7, 8
43.	Kaempferol 3-*O*-rutinoside[a]	$C_{27}H_{30}O_{16}$	609.1461	609.1478 (100), 285.0407 (61.6), 284.0331 (23.6), 255.0301 (26.5), 227.0348 (16.6), 151.0027 (3.3), 135.0078 (1.2), 107.0124 (2.6)	5.06	2.827	2, 3, 4, 7, 8

(Continues)

TABLE 2 (Continued)

No	Identified/tentatively annotated compound	Molecular formula	Exact mass [M-H]$^-$	Fragmentation pattern in (-) ESI-MS/MS	t_R (min)	Δ ppm	Distribution
44.	Nepetin 7-*O*-deoxyhexosyl-hexoside	$C_{28}H_{32}O_{16}$	623.1618	623.1638 (100), 315.0493 (7.9), 314.0438 (69.8), 300.0268 (8.3), 299.0201 (48.2), 271.0251 (23.6), 253.0506 (3.4), 165.9897 (9.2), 164.9819 (3.91), 136.9871 (0.9), 133.0283 (5.3),	5.12	3.213	4
45.	Hyperoside[a]	$C_{21}H_{20}O_{12}$	463.0882	463.0892 (100), 301.0353 (33.8), 300.0279 (75.8), 271.0251 (35.4), 255.0299 (15.5), 227.0345 (1.9), 178.9977 (2.2), 151.0025 (5.8), 121.0280 (1.2), 107.0125 (2.4)	5.18	2.096	1, 2, 3, 4, 5, 6, 7, 8
46.	Isorhamnetin 3-*O*-dihexoside	$C_{28}H_{32}O_{17}$	639.1567	639.1587 (97.6), 315.0516 (100), 300.0279 (14.7), 271.0251 (29.6), 227.0345 (4.0), 151.0025 (3.8), 107.0125 (0.9)	5.24	3.156	2, 3, 4
47.	Kaempferol 3-*O*-hexosyl-7-*O*-deoxyhexoside	$C_{27}H_{30}O_{15}$	593.1512	593.1526 (100), 431.0984 (2.4), 285.0392 (14.9), 284.0330 (94.0), 255.0300 (47.3), 227.0348 (28.8), 211.0394 (1.4), 151.0026 (2.0), 135.0073 (0.5), 107.0124 (1.4)	5.26	2.355	3, 4, 5, 6, 7, 8
48.	Isoquercitrin[a]	$C_{21}H_{20}O_{12}$	463.0882	463.0892 (100), 301.0353 (43.3), 300.0279 (77.5), 271.0250 (41.8), 255.0298 (17.8), 227.0348 (2.7), 211.0395 (1.3), 178.9984 (3.4), 151.0023 (5.8), 121.0278 (1.2), 107.0122 (2.8)	5.29	2.096	1, 2, 3, 4, 7, 8
49.	Nepetin 7-*O*-pentosylhexoside	$C_{27}H_{30}O_{16}$	609.1461	609.1475 (100), 315.0514 (32.2), 314.0437 (23.9), 300.0277 (35.7), 299.0201 (22.7), 271.0256 (26.8), 255.0297 (15.0), 243.0294 (6.4), 215.0346 (6.8), 199.0393 (2.2), 165.9897 (4.2), 133.0280 (2.3), 109.9996 (1.1)	5.32	2.318	2, 3, 4
50.	Isorhamnetin 4′-*O*-rutinoside	$C_{28}H_{32}O_{16}$	623.1618	623.1633 (100), 315.0502 (14.9), 314.0438 (92.0), 299.0203 (21.1), 271.0251 (22.6), 255.0297 (6.6), 243.0297 (20.4), 227.0353 (5.5), 151.0026 (4.2), 107.0124 (2.5)	5.39	2.523	3, 4, 5
51.	Isorhamnetin 3-*O*-pentosylhexoside	$C_{27}H_{30}O_{16}$	609.1461	609.1479 (100), 315.0516 (82.5), 300.0280 (13.4), 299.0199 (11.1), 271.0251 (26.7), 227.0349 (3.5), 151.0349 (3.5)	5.48	3.024	2, 3, 4
52.	Luteolin 7-*O*-rutinoside[a]	$C_{27}H_{30}O_{15}$	593.1501	593.1528 (100), 285.0407 (73.42), 284.0330 (43.8), 255.0299 (32.8), 227.0345 (20.1), 211.0401 (2.5), 151.0027 (2.9), 107.0125 (0.9)	5.63	2.759	1, 2, 3, 4, 6
53.	Isorhamnetin 3-*O*-rutinoside[a]	$C_{28}H_{32}O_{16}$	623.1618	623.1635 (100), 315.0515 (82.9), 314.0439 (33.0), 299.0201 (11.9), 271.0252 (24.3), 255.0301 (9.5), 243.0298 (15.9), 227.0344 (4.1), 151.0024 (3.22), 107.0126 (0.6)	5.79	2.715	2, 3, 4

(Continues)

TABLE 2 (Continued)

No	Identified/tentatively annotated compound	Molecular formula	Exact mass [M-H]$^-$	Fragmentation pattern in (-) ESI-MS/MS	t_R (min)	Δ ppm	Distribution
54.	Kaempferol 3-*O*-glucoside[a]	$C_{21}H_{20}O_{11}$	447.0933	447.0941 (100), 285.0400 (23.4), 284.0328 (59.1), 255.0299 (48.0), 227.0347 (46.4), 211.0126 (1.7), 151.0027 (2.0), 135.0071 (2.0), 107.0126 (0.7)	5.84	1.734	1, 2, 3, 4, 5, 6, 8
55.	Quercitrin[a]	$C_{21}H_{20}O_{11}$	447.0933	447.0942 (100), 301.0354 (58.1), 300.0279 (64.6), 271.0250 (32.8), 255.0300 (16.2), 211.0404 (1.7), 178.9977 (4.1), 151.0026 (7.9), 121.0281 (2.5), 107.0125 (3.6)	5.93	2.137	1, 2, 3, 4, 5, 6, 8
56.	Isorhamnetin 3-*O*-glucoside[a]	$C_{22}H_{22}O_{12}$	477.1039	477.1047 (100), 315.0501 (10.2), 314.0438 (50.9), 300.0278 (1.8), 271.0250 (19.6), 243.0299 (22.9), 151.0028 (2.8), 107.0121 (0.6)	6.00	1.867	1, 2, 3, 4, 5, 6, 7, 8
57.	Luteolin 7-*O*-glucoside[a]	$C_{21}H_{20}O_{11}$	447.0933	447.0942 (32.4), 285.0406 (100), 284.0332 (4.1), 257.0455 (1.5), 241.0509 (0.9), 217.0503 (1.3), 151.0026 (7.9), 133.0282 (10.6), 107.0125 (3.8)	6.05	2.137	1, 2, 3, 4, 5, 6, 7, 8
58.	Apigenin 7-*O*-glucoside[a]	$C_{21}H_{20}O_{10}$	431.0973	431.0991 (80.3), 269.0456 (100), 268.0379 (61.7), 267.0309 (0.9), 240.0420 (6.1), 211.0405 (1.1), 151.0028 (3.6), 117.0335 (3.0), 107.00124 (2.9)	6.13	1.670	1, 2, 3, 4, 5, 6, 7, 8
59.	3′-Hydroxyflavone 4′-*O*-dihexoside	$C_{27}H_{30}O_{14}$	577.1563	577.1578 (35.5), 253.0506 (100), 255.0562 (1.8), 209.0603 (4.2), 161.0443 (0.3), 133.0282 (33.5), 117.0331 (0.8)	6.16	2.601	2, 3, 4
60.	3′-Hydroxyflavone 4′-*O*-hexoside	$C_{21}H_{20}O_9$	415.1035	415.1045 (0.2), 253.0506 (100), 240.9953 (0.1), 225.0553 (1.6), 197.0606 (0.5), 133.0282 (32.6), 117.0331 (1.2)	6.24	2.565	1, 2, 3, 4, 5, 6, 7, 8
61.	Flavone 4′-*O*-dihexoside	$C_{27}H_{30}O_{13}$	561.1614	607.1675 (1.1) ([M-H]$^-$+CH_2O_2), 561.162 (6.8), 237.0554 (100), 238.0590 (5.8), 209.0604 (5.9), 161.0234 (0.6), 117.0332 (25.2), 93.0330 (0.2)	6.45	2.737	2, 3, 4
62.	4-Hydroxy-3′-methoxyflavone 7-*O*-hexoside	$C_{22}H_{22}O_{10}$	445.1140	445.1149 (81.3), 283.0614 (100), 268.0379 (78.8), 240.0426 (12.5), 211.0396 (0.8), 167.0495 (0.3), 148.0154 (4.7), 133.0280 (0.4)	6.46	1.910	2, 3, 4
63.	3′,4′,5′-Trihydroxyflavone	$C_{15}H_{10}O_5$	269.0456	269.0456 (100), 251.0349 (0.1), 241.0503 (0.4), 223.0403 (1.1), 149.0231 (44.1), 117.0333 (0.8), 105.0329 (0.8)	6.64	0.161	1, 2, 3, 4, 5
64.	Flavone 4′-*O*-hexoside	$C_{21}H_{20}O_8$	399.1085	445.1148 (18.6) ([M-H]$^-$+CH_2O_2), 399.1088 (5.8), 237.0556 (100), 207.0499 (0.5), 117.0332 (9.7)	6.73	0.650	1, 2, 3, 4, 5, 6, 7, 8
65.	Luteolin[a]	$C_{15}H_{10}O_6$	285.0405	285.0406 (100), 257.0441 (0.2), 243.0296 (0.6), 217.0504 (0.8), 151.0026 (4.2), 133.0282 (21.3), 107.0125 (3.8), 121.0284 (0.9)	7.57	0.452	1, 2, 4, 5, 7

(Continues)

TABLE 2 (Continued)

No	Identified/tentatively annotated compound	Molecular formula	Exact mass [M-H]$^-$	Fragmentation pattern in (-) ESI-MS/MS	t_R (min)	Δ ppm	Distribution
66.	Quercetin[a]	$C_{15}H_{10}O_7$	301.0354	301.0356 (100), 273.0413 (3.3), 257.0457 (1.9), 201.0559 (0.5), 178.9977 (23.0), 151.0025 (50.2), 149.0235 (2.9)121.0281 (13.8), 107.0123 (15.3)	7.58	0.877	1, 2, 3, 4, 5
67.	3′,4′-Dihydroxyflavone	$C_{15}H_{10}O_4$	253.0506	253.0505 (100), 235.0398 (0.2), 225.0550 (1.4), 209.0606 (1.1), 181.0648 (0.4), 133.0281 (54.4), 117.0332 (2.2), 105.0329 (0.2)	7.94	−0.601	1, 2, 3, 4, 5, 6, 7, 8
68.	4′,7-Dihydroxy-3′-dimethoxyflavone	$C_{16}H_{12}O_5$	283.0612	283.0614 (23.4), 268.0379 (100), 240.0428 (7.0), 211.0399 (0.9), 148.0155 (10.5)	7.95	0.718	1, 2, 3, 4, 5, 6, 7, 8
69.	Apigenin[a]	$C_{15}H_{10}O_5$	269.0456	269.0457 (100), 225.0556 (1.9), 201.0552 (0.9), 151.0026 (5.3), 149.0233 (4.8), 117.0332 (20.1), 107.0125 (5.4)	8.60	0.496	1, 2, 3, 4
70.	Kaempferol[a]	$C_{15}H_{10}O_6$	285.0405	285.0406 (100), 257.0468 (0.8), 239.0353 (1.1), 229.0504 (1.0), 211.0399 (0.9), 201.0555 (0.6), 151.0025 (1.2), 161.0237 (0.7), 135.0075 (0.5), 107.0125 (1.0)	8.81	0.452	1, 2, 5, 7
71.c	Chrysoeriol[a]	$C_{16}H_{12}O_6$	299.0561	299.0563 (100), 284.0329 (81.8), 256.0378 (16.7), 239.0354 (0.3), 227.0346 (2.5), 211.0390 (0.8), 151.0023 (2.9), 134.0359 (0.9), 125.0230 (0.2), 107.0126 (2.2)	8.93	0.765	1, 2, 3, 4, 5, 6, 7
72.	Isorhamnetin[a]	$C_{15}H_{14}O_7$	315.0499	315.0516 (100), 301.0316 (3.4), 300.0279 (44.2), 271.0248 (2.7), 243.0302 (1.2), 227.0343 (1.2), 163.0022 (2.6), 151.0024 (8.4), 107.0124 (7.1)	9.11	1.727	1, 2, 3
73.	4′-Hydroxyflavone	$C_{15}H_{10}O_3$	237.0557	237.0554 (100), 209.0604 (1.5), 193.0554 (0.9), 117.0331 (50.8), 104.0188 (0.1)	9.42	−1.339	1, 2, 3, 4, 5, 6, 7, 8
74.	7-*O*-Methylluteolin	$C_{15}H_{10}O_3$	299.0561	299.0564 (100), 284.0329 (68.0), 227.0360 (2.1), 211.0398 (3.2), 201.0182 (2.7), 151.0029 (1.5), 133.0282 (10.9)	9.54	0.965	1, 2

Note: 1: aerial parts—EA; 2: aerial parts—EtOH; 3: aerial parts—EtOH/water; 4: aerial parts—water; 5: rhizomes—EA; 6: rhizomes—EtOH; 7: rhizomes—EtOH/water; 8: rhizomes—water.

[a]Compare to reference standards.

suggesting a strong link between flavonoid content and DPPH scavenging ability. Meanwhile, the lowest MCA value among the aerial parts extracts was observed in the water extract at 35.43 mg EDTAE/g, despite this extract showing a comparatively low TPC and TFC. For the rhizomes, the ethanol extract showed the highest antioxidant activity in the DPPH assay with a value of 49.63 mg TE/g, while the lowest value in the EA extract was 36.18 mg TE/g. The ethanol/water extract showed the highest CUPRAC value at 115.07 mg TE/g, emphasizing its exceptional antioxidant potential, possibly due to the highest phenolic compound as suggested by its high TPC in the Table 1. The varying antioxidant activity across both parts of the plant depending on the solvent used for extraction, with ethanol and ethanol/water mixtures generally exhibiting higher antioxidant activities. This variance could be due to the different polarities of the solvents, affecting the solubility of various antioxidant compounds. The ethanol/water mixture, in particular, seems to provide a balanced medium that efficiently extracts both phenolic and flavonoid compounds, thereby enhancing the antioxidant capacity of the extracts. In comparison to the TPC and TFC data (Table 1), there appears to be a general correlation where extracts with higher phenolic and flavonoid contents tend to exhibit

TABLE 3 Antioxidant effects of *Primula vulgaris* extracts.

Parts	Solvent	DPPH (mg TE/g)	ABTS (mg TE/g)	CUPRAC (mg TE/g)	FRAP (mg TE/g)	PBD (mmol TE/g)	MCA (mg EDTAE/g)
Aerial parts	EA	4.65 ± 0.05^{h}	26.90 ± 0.26^{e}	82.93 ± 1.93^{b}	35.20 ± 0.29^{e}	1.74 ± 0.08^{a}	24.94 ± 1.37^{d}
	Ethanol	17.21 ± 0.19^{g}	27.97 ± 1.25^{e}	84.44 ± 1.78^{b}	40.91 ± 0.87^{c}	1.87 ± 0.04^{a}	29.74 ± 0.60^{c}
	Ethanol/water	39.89 ± 0.62^{d}	41.78 ± 0.33^{c}	65.34 ± 0.24^{c}	42.78 ± 0.12^{c}	1.12 ± 0.03^{c}	33.20 ± 0.25^{b}
	Water	32.40 ± 0.15^{f}	37.13 ± 0.23^{d}	42.92 ± 0.59^{d}	32.59 ± 0.56^{f}	0.84 ± 0.01^{d}	35.43 ± 0.24^{a}
Rhizomes	EA	36.18 ± 0.08^{e}	41.35 ± 0.20^{c}	86.47 ± 1.92^{b}	38.34 ± 1.89^{d}	1.48 ± 0.09^{b}	18.95 ± 0.54^{e}
	Ethanol	49.63 ± 0.05^{a}	50.88 ± 0.05^{a}	84.84 ± 2.66^{b}	57.50 ± 0.39^{b}	1.08 ± 0.03^{c}	2.23 ± 0.12^{g}
	Ethanol/water	48.81 ± 0.08^{b}	50.89 ± 0.07^{a}	115.07 ± 1.71^{a}	79.11 ± 0.45^{a}	1.80 ± 0.04^{a}	11.81 ± 0.06^{f}
	Water	46.16 ± 0.07^{c}	49.05 ± 0.45^{b}	60.71 ± 1.94^{c}	35.75 ± 0.29^{e}	1.12 ± 0.07^{c}	23.78 ± 0.85^{d}

PBD: phosphomolybdenum; MCA: metal chelating; TE: trolox equivalent; EDTAE: EDTA equivalent.
Note: Values are reported as mean ± SD of three parallel experiments. Different letters$^{(a\text{-}h)}$ indicate significant differences between the tested extracts ("a" indicate the highest ability, $p < .05$).

TABLE 4 Enzyme inhibitory effects of *Primula vulgaris* extracts.

Parts	Solvent	AChE (mg GALAE/g)	BChE (mg GALAE/g)	Tyrosinase (mg KAE/g)	Amylase (mmol ACAE/g)	Glucosidase (mmol ACAE/g)
Aerial parts	EA	2.48 ± 0.07^{c}	3.05 ± 0.07^{a}	1.07 ± 0.17^{d}	1.64 ± 0.02^{a}	0.49 ± 0.02^{c}
	Ethanol	1.88 ± 0.29^{d}	2.06 ± 0.07^{b}	50.03 ± 1.02^{b}	1.07 ± 0.04^{c}	0.48 ± 0.07^{c}
	Ethanol/water	2.53 ± 0.02^{bc}	0.36 ± 0.04^{e}	31.08 ± 0.90^{c}	0.41 ± 0.01^{e}	0.63 ± 0.07^{b}
	Water	0.21 ± 0.01^{e}	0.24 ± 0.04^{e}	na	0.18 ± 0.01^{g}	na
Rhizomes	EA	2.51 ± 0.02^{bc}	1.04 ± 0.09^{d}	50.34 ± 1.35^{b}	1.26 ± 0.01^{b}	0.64 ± 0.04^{b}
	Ethanol	2.86 ± 0.02^{a}	3.00 ± 0.07^{a}	57.56 ± 1.03^{a}	0.57 ± 0.01^{d}	0.76 ± 0.01^{a}
	Ethanol/water	2.78 ± 0.01^{ab}	1.84 ± 0.07^{c}	57.02 ± 0.52^{a}	0.53 ± 0.01^{d}	na
	Water	0.23 ± 0.04^{e}	0.22 ± 0.04^{e}	na	0.26 ± 0.01^{f}	0.83 ± 0.01^{a}

GALAE: galanthamine equivalent; KAE: kojic acid equivalent; ACAE: acarbose equivalent; na: not active.
Note: Values are reported as mean ± SD of three parallel experiments. Different letters$^{(a-g)}$ indicate significant differences between the tested extracts ("a" indicate the highest ability, $p < .05$).

greater antioxidant activities. However, this relationship is not strictly linear, as seen with the water extract from the aerial parts and rhizomes, which had lower TPC and TFC values but showed relatively high antioxidant activity in MCA 35.43 mg EDTAE/g and 23.78 mg EDTAE/g, respectively. This suggests that other factors, such as the presence of specific compounds with strong antioxidant activities that are not measured by TPC and TFC assays, might also play a significant role. The antioxidant activity observed in our investigation differs from that of *Primula* aqueous ethanol extracts, which exhibited an activity of 86.65% (Jurca et al., 2015). According to the findings of Demir et al. (2019), the extract derived from *P. vulgaris* flowers using dimethyl sulfoxide exhibits significant antioxidant properties.

3.4 | Enzyme inhibition activity

The enzyme inhibition activities of *P. vulgaris* extracts were measured against acetylcholinesterase (AChE), butyrylcholinesterase (BChE), tyrosinase, α-amylase, and α-glucosidase (Table 4). The water extract from aerial parts exhibited the minimal AChE inhibition activity at 0.21 mg GALAE/g, whereas the aerial ethanol/water extract demonstrated the maximum activity with 2.53 mg GALAE/g. Additionally, in the current study, the aerial parts' EA extract displayed superior BChE inhibition efficiency 3.05 mg GALAE/g. Consistent with previous research, the ethanol and hydroalcoholic extracts of *P. auriculata's* aerial parts and rhizomes have demonstrated significant inhibitory effects on AChE, while the ethyl acetate extract specifically exhibited the strongest activity against BChE, with an impact of 3.54 mg GALAE/g dry extract (Kurt-Celep et al., 2022). This suggests that the extraction solvent significantly influences the extract's ability to inhibit specific enzymes. Mahran et al. (2019) discovered that leaf extract from *P. boveana*, which contains flavone, was identified as being half as effective as an AChE inhibitor.

Interestingly, the ethanol extract exhibited a notably high tyrosinase inhibition activity at 50.03 mg KAE/g, contrasting with its relatively lower AChE 1.88 mg GALAE/g and BChE 2.06 mg GALAE/g inhibition activities. This high tyrosinase inhibition correlates with its substan-

tial antioxidant activity and TPC, indicating the presence of specific phenolic compounds that are effective in both antioxidant activity and enzyme inhibition. Previous studies claimed that extracts with an alcoholic or hydroalcoholic base exhibit superior tyrosinase inhibition capabilities (Acquaviva et al., 2023; Nilofar et al., 2024). Similarly, another finding reveal that both the aerial parts and rhizomes of *P. auriculata* ethanol and hydroethanolic extracts demonstrate enhanced anti-tyrosinase activity, with measurements ranging from 67.94 mg KAE/g to 76.36 mg KAE/g. The observed increase in variation in activity noted in the current study may be attributed to species-specific differences (Kurt-Celep et al., 2022).

For the rhizomes, ethanol extraction resulted in the highest AChE inhibition activity measuring 2.86 mg GALAE/g, and similarly high BChE 3.00 mg GALAE/g and tyrosinase 57.56 mg GALAE/g inhibition activities. Water extracts showed the lowest enzyme inhibition activities for AChE and BChE, highlighting again the impact of solvent choice on the bioactivity of the extracts. The α-glucosidase inhibition by water extract was the highest among rhizome extracts at 0.83 mmol ACAE/g, contrasting with its low enzyme inhibition activities elsewhere. The EA extracts from both parts of *P. vulgaris* demonstrated enhanced α-amylase inhibition activity, targeting the α-glucose-digesting enzyme, whereas the water extracts exhibited lower activity in this regard. The α-glucosidase inhibition by water extract was the highest among rhizome extracts at 0.83 mmol ACAE/g, contrasting with its low enzyme inhibition activities elsewhere. Moreover, all the extracts showed relatively low anti-α-glucosidase inhibition capabilities. In a closely related study, Kurt-Celep et al. (2022) conducted comprehensive research examining the effects of extracts from both the aerial and underground parts of plants within the *Primula* genus. Their findings revealed that these extracts of *P. auriculata* exhibit a notable decrease in the inhibition of α-amylase and α-glucosidase enzymes (Kurt-Celep et al., 2022). This study, which extends our understanding of the pharmacological properties of the *Primula* genus, demonstrates the potential variability in bioactive compounds across different parts of the same plant species, contributing valuable insights into their medicinal and therapeutic applications. Moreover, certain extracts like ethanol/water extract may contain specific bioactive compounds that are particularly effective against one type of enzyme but not others, suggesting a selective inhibition mechanism that could be beneficial for therapeutic applications targeting specific enzymes.

3.5 | Molecular docking

Molecular docking was conducted for the tested enzymes and proteins involved in the inflammation process. The coordinates and grid sizes required for these analyses are provided in Supplementary Material 1 and 3. From the numerous compounds detected in *Primula*, nine were selected for in-depth analyses due to their widespread distribution. These selected compounds exhibited binding energies ranging from −10.2 to −4.5 kcal/mol with enzymatic targets and proteins associated with inflammation (Supplementary Material 2 and 4). A minimum docking score threshold of −8 or lower was set for investigations, and these compounds were evaluated in detail. The binding energies and interacting residues are presented in Tables 5 and 6, and a visual representation is provided in Figure 1.

The results of the molecular docking study, conducted with nine molecules, indicated that the binding energies observed for the examined enzymes were notably highest than expected. In contrast, only four compounds, namely 4′-Hydroxyflavone, isoquercitrin, primulaverin, and primeverin, demonstrated significant binding energies toward enzymes and proteins. The analysis of binding energies concerning protein and enzyme residues revealed notable interactions between MMP-9 and 4′-Hydroxyflavone, NF-κB and primulaverin, AChE and isoquercitrin, AChE and gaultherin, and AChe and primverin (Tables 5 and 6, Figure 1). Hydrogen bonds played a dominant role in these interactions, as evidenced by the number of hydrogen bonds identified in the interactions between AChE and gaultherin (10) and between AChE and primverin (8). The highest docking score, −10.2 kcal/mol, was recorded for the interaction with AChe, which highlights isoquercitrin as exhibiting the most potent inhibitory effect among the compounds studied.

The study revealed that multiple compounds exhibited repeated interactions with unique amino acid residues that interact with enzymes BChE, amylase, AChE, NF-κB, and MMP-9. For example, residue GLU A:197 was utilized by multiple compounds in the interaction between NF-κB and isoquercitrin, primulaverin, and primverin; GLN A:63 with amylase; and LEU A:188 with MMP-9. In AChE, residues such as GLY A:120 and GLY A:121 were repeatedly interacted with by three different compounds. The interaction of these residues with multiple compounds suggests that they play a critical role in enzyme binding processes and are therefore potential therapeutic targets (Tables 5 and 6). It has been observed that the compounds Ache primverin, isoquercitrin, and gaultherin exhibit notably low binding energies with acetylcholinesterase (AChE). It is noteworthy that primverin and gaultherin have demonstrated the ability to form pi-sigma interactions with PHE A:338 and pi–pi interactions with TRP A:86 within the AChE enzyme. These interactions may contribute to their inhibitory activity, thereby underscoring the significance of these compounds in the design of Alzheimer's disease therapies (Figure 1a and c) (McGleenon et al., 1999). A comprehensive analysis of the interactions between the MMP-9 protein and 10 distinct ligands revealed the involvement of specific residues, including LEU A:397, LEU A:188, and ALA A:189. However, the presence of a specific residue, such as TYR A:423, was not observed. Notably, the 4′-Hydroxyflavone ligand demonstrated a remarkable binding affinity (−8.9 kcal/mol) with these residues (Basavarajappa et al., 2023). Conversely, the observed binding energy of −8.3 kcal/mol for primulaverine interacting with NF-κB, with two interactions at ASP A:964 and also with the residue ASN A:951, is noteworthy when compared with the literature. ASN A:951 was found to be specific and compatible for this molecule (Suhail et al., 2023). Primulaverine demonstrated a high binding energy of −8.7 kcal/mol with HAase and interacted with crucial residues, including TRP A:141 (2), ASP A:142, TYR A:261, TYR A:247, and SER A:245 (Table 5).

TABLE 5 The docking score (kcal/mol) and interacting residues of the enzyme.

Compound	Receptor		Binding energy (kcal/mol)	Interaction	Amino acid residues	
	Target enzyme	PDB ID		Type	Number	Binding site
4′-Hydroxyflavone	AChE	2Y2V	−9.5	Hydrogen bond	2	GLY A:122, GLY A:121
Gaultherin	AChE	2Y2V	−9.5	Hydrogen bond	10	GLY A:120 (2) GLU A:202 (2), TYR A.233, GLY A:121, GLY A:122, HIS A:447, TYR A:124 (2)
Isoquercitrin	AChE	2Y2V	−10.2	Hydrogen bond	4	GLU A:202, HIS A:447, TYR A124, ASP A:74, ASN A:87,
Pirmulaverin	AChE	2Y2V	−9.5	Hydrogen bond	6	ASP A:74, ARG A:196, PHE A:295, GLU A:202, ALA A:204, GLY A:120
Primeverin	AChE	2Y2V	−9.6	Hydrogen bond	8	GLY A:120, TYR A:133 (2), GLY A:121, ALA A:204, GLY A:122, HIS A:447, TYR A:124,
Roseoside	AChE	2Y2V	−9.2	Hydrogen bond	3	TYR A:124, PHE A:295, ARG A:296
4′-hydroxyflavone	Amylase	2QV4	−9.1	Hydrogen bond	2	ASP A:197, GLN A:63
Gaultherin	Amylase	2QV4	−8.1	Hydrogen bond	4	GLU A:233 (2) HIS A:201, GLN A:63
Isoquercitrin	Amylase	2QV4	−8.1	Hydrogen bond	6	TRP A:59, GLN A:63, HIS A:305, ASP A:197, HIS A:299, GLU A:233
Pirmulaverin	Amylase	2QV4	−8.4	Hydrogen bond	5	GLN A:63 (2), ASP A:300, ASP A:197, GLU A:233,
Primeverin	Amylase	2QV4	−8.3	Hydrogen bond	5	ARG A:195, ASP A:300 GLU A:233, TRP A:59, THR A:163,
4′-hydroxyflavone	BChE	3DJY	−8.5	Hydrogen bond	2	ASN A:68, ASP A:70
Gaultherin	BChE	3DJY	−8.7	Hydrogen bond	2	GLY A:116, HIS A:438
Isoquercitrin	BChE	3DJY	−9.9	Hydrogen bond	4	TYR A:128, HIS A:438, GLU A:197, SER A:287
Pirmulaverin	BChE	3DJY	−8.6	Hydrogen bond	5	GLU A:197 (2), ALA A:199, GLY A:117, SER A:287
Primeverin	BChE	3DJY	−9.1	Hydrogen bond	4	GLY A:117, GLU A:197, ALA A:199 (2)
Roseoside	BChE	3DJY	−8.5	Hydrogen bond	3	GLY A:116, TRP A:82, LEU A:286
Isoquercitrin	HAase	2PE4	−8.7	Hydrogen bond	6	TRP A:141 (2) ASP A:142, TYR A:261, TYR A:247, SER A:245
Isoquercitrin	Collagenase	1CGL	−8.5	Hydrogen bond	2	HIS A:218, ASN A:180

3.6 | Molecular dynamics (MD) simulations of docked complexes

The aim of this study is to identify potential therapeutic agents by meticulously examining the interactions occurring at the molecular level between ligands and the target proteins to which they are bound. A comprehensive analysis was conducted on nine potential ligands to evaluate their biological potency and capacity for protein interaction. The ligands were selected based on their molecular docking scores. Primulaverin for NF-κB, 4′-Hydroxyflavone for MMP-9, and isoquercitrin for hyaluronidase were selected based on their substantial interaction metrics, as evidenced by in vitro analysis. These ligands

TABLE 6 The docking score (kcal/mol) and interacting residues of the protein.

Compound	Receptor		Binding energy (kcal/mol)	Interaction	Amino acid residues	
	Target protein	PDB ID		Type	Number	Binding site
4′-Hydroxyflavone	MMP-9	1GKC	−8.6	Hydrogen bond	4	TYR A:423, LEU A:397, LEU A:188, ALA A:189
Isoquercitrin	MMP-9	1GKC	−8.2	Hydrogen bond	6	HIS A:405, GLU A:402, ALA A:188, HIS A:401, LEU A:188, TYR A:423
Pirmulaverin	MMP-9	1GKC	−8.5	Hydrogen bond	1	ARG A:424
Primeverin	MMP-9	1GKC	−8.5	Hydrogen bond	3	HIS A:405, LEU A:188, ALA A:189,
Isoquercitrin	NF-κB	4fa6	−8.0	Hydrogen bond	5	ASP A:950, LYS A:807 (2), ASP A:964, LYS A:833
Pirmulaverin	NF-κB	4fa6	−8.3	Hydrogen bond	3	ASP A:964 (2), ASN A:951
Primeverin	NF-κB	4fa6	−8.0	Hydrogen bond	2	ASP A:950, ASN A:951

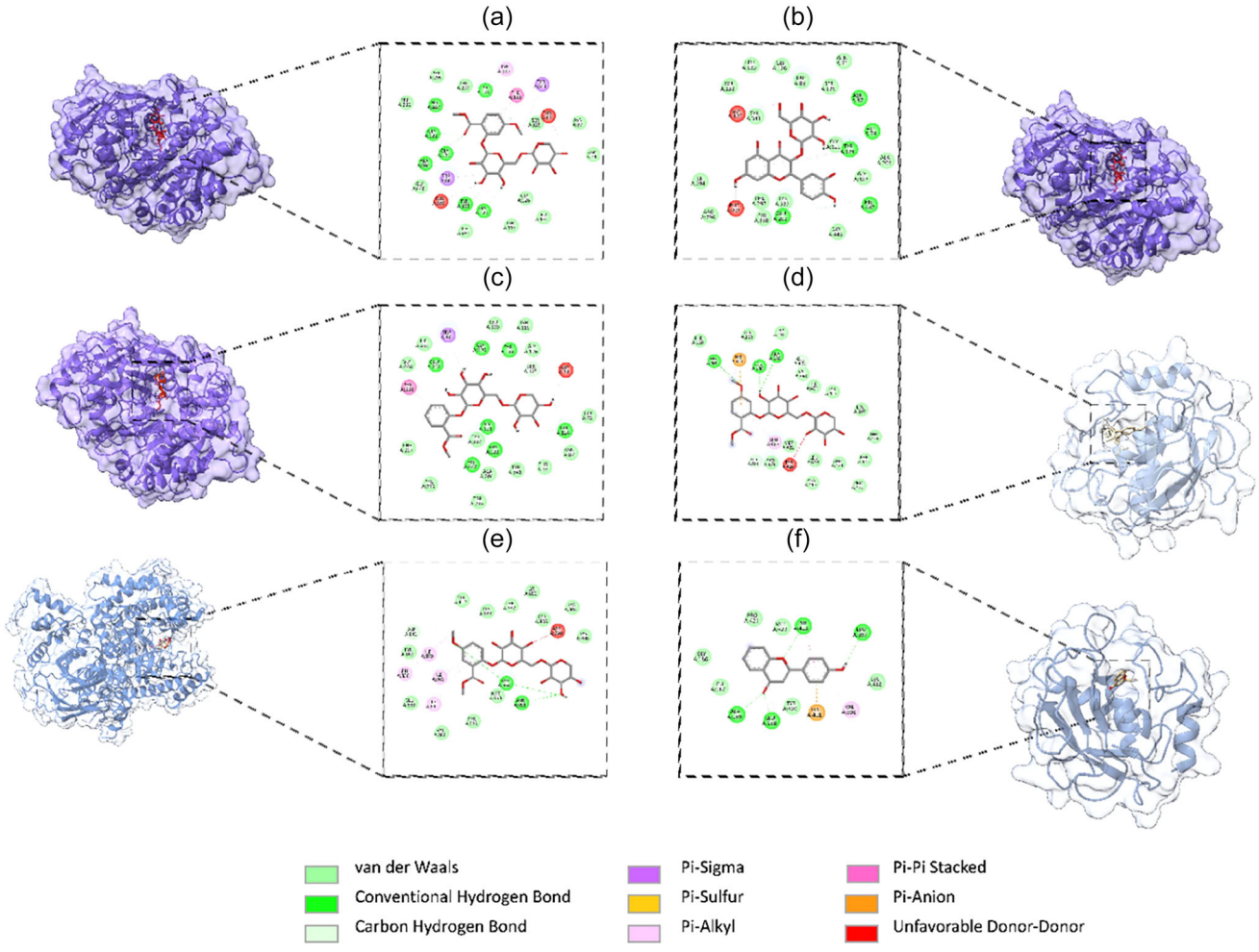

FIGURE 1 Enzymes and proteins' active sites with compounds showing the best binding energy: (a) interaction between AChe and primeverin; (b) interaction between AChe and isoquercitrin; (c) interaction between AChe and gaultherin; (d) interaction between MMP9 and primeverin; (e) interaction between NF-κB and pirmulaverin; (f) interaction between MMP9 and a 4′-hydroxyflavone.

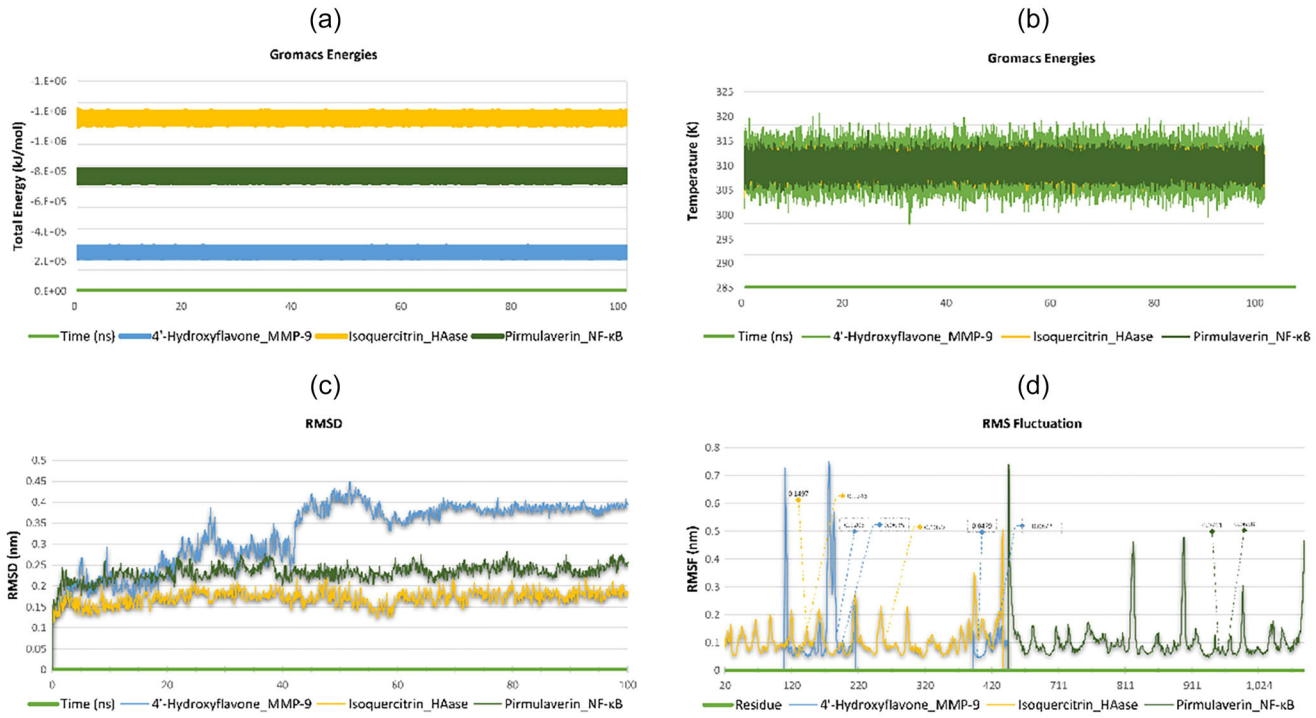

FIGURE 2 Presentation of molecular dynamics simulations in graphical form: (a) total energy of MMP-9, HAase, and NF-κB in complex with bioactive molecules: 4′-hydroxyflavone, isoquercitrin, and pirimulaverin; (b) temperature of MMP-9, HAase, and NF-κB in complex with bioactive molecules: 4′-hydroxyflavone, isoquercitrin, and pirimulaverin; (c) RMSD of MMP-9, HAase, and NF-κB in complex with bioactive molecules: 4′-hydroxyflavone, isoquercitrin, and pirimulaverin; (d) RMSF of MMP-9, HAase, and NF-κB in complex with bioactive molecules: 4′-hydroxyflavone, isoquercitrin, and pirimulaverin..

have been identified as essential for molecular dynamics (MD) simulations, distinguished by their specificity and the stability of their interactions with the target proteins.

The temperature profiles of all three complexes remained constant within the physiological range with small fluctuations around the 300 K target temperature, indicating that the simulations reached thermal equilibrium. In addition, Gromacs energy analyses (Figure 2a) revealed that following the initial equilibration phase, the energy levels for each complex remained continuous and constant. This constancy indicates that the simulated protein–ligand interactions show a high structural and thermodynamic stability under physiological conditions, indicating that the simulation results are biologically reliable and reproducible (Figure 2b). The RMSD Plot shows how the RMSD changes over time for each ligand. For example, the RMSD values of 4′-Hydroxyflavone and Isoquercitrin follow a relatively lower and stable trend, while MMP-9 and Primulaverin_NF-kB show a higher and fluctuating RMSD profile. This indicates that 4′-Hydroxyflavone and Isoquercitrin form more stable complexes with specific protein targets and these complexes are structurally less altered (Figure 2c). The RMSF plot indicates that certain regions of the protein show greater flexibility in response to ligand binding. The graph shows that 4′-Hydroxyflavone and Primulaverine_NF-kB show distinct peaks in some regions. These peaks indicate that the ligands induce high levels of conformational changes in these regions of the protein and that these areas are potentially critical for ligand binding (Figure 2d).

Molecular dynamics simulations are vital in understanding the dynamic behavior and ligand binding efficiency of specific amino acid residues in protein–ligand complexes. In this study, RMSF analyses on 4′-Hydroxyflavone_MMP-9, Isoquercitrin_HAase and Primulaverin_NF-κB complexes clearly reveal the flexibility and stability of the residues in the interaction with ligands. In particular, in the 4′-Hydroxyflavone_MMP-9 complex, the low RMSF values of residues LEU A:188 (0.1203 nm), ALA A:189 (0.0635 nm), LEU A:397 (0.0479 nm), and TYR A:423 (0.0872 nm) indicate that these amino acids establish stable interactions with the ligand and contribute to the overall stability of the complex. In the Isoquercitrin_HAase complex, the relatively high RMSF values of the TRP A:141 (0.1246 nm) and ASP A:142 (0.1497 nm) residues indicate that these moieties show high flexibility in response to ligand binding, while the TYR A:261 (0.1059 nm) residue exhibits a relatively stable structure with a lower value. In the primulaverine_NF-κB complex, the RMSF values of residues ASP A:964 (0.0658 nm) and ASN A:951 (0.0761 nm) emphasize the important roles and interaction dynamics of these amino acids in ligand binding. Analysis of these residues contributes to a better understanding and targeting of these interaction points as potential targets in drug design and development processes. These data are an important resource for understanding the structural dynamics of protein–ligand complexes in detail and identifying potential sites to target in the drug development process.

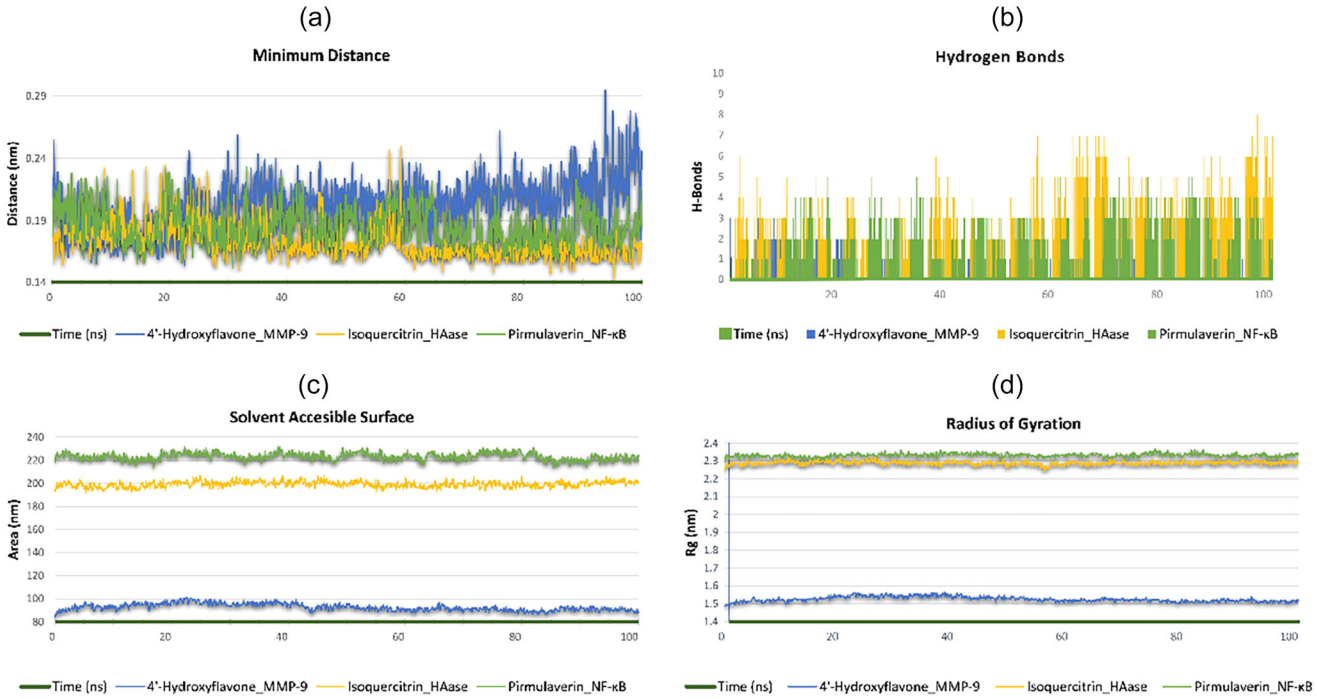

FIGURE 3 Presentation of molecular dynamics simulations in graphical form: (a) minimum distance of MMP-9, HAase, and NF-κB in complex with bioactive molecules: 4'-Hydroxyflavone, isoquercitrin, and pirimulaverin; (b) hydrogen bond of MMP-9, HAase, and NF-κB in complex with bioactive molecules: 4'-Hydroxyflavone, isoquercitrin, and pirimulaverin; (c) solvent accessibility of MMP-9, HAase, and NF-κB in complex with bioactive molecules: 4'-Hydroxyflavone, isoquercitrin, and pirimulaverin; (d) radius of gyration of MMP-9, HAase, and NF-κB in complex with bioactive molecules: 4'-Hydroxyflavone, isoquercitrin, and pirimulaverin.

Molecular dynamics simulations are an important tool in understanding the dynamics of hydrogen bonding and minimum distances of protein–ligand complexes. The data obtained from these simulations reveal that the 4′-Hydroxyflavone and MMP-9 complex forms zero hydrogen bonds at minimum and three hydrogen bonds at maximum during the simulation, fluctuations are observed from time to time and 100 ns of full protein simulation results in no hydrogen bonds. The complex of isoquercitrin and HAase reached a maximum of nine hydrogen bonds and generally maintained three hydrogen bonds. The primulaverine and NF-κB complex consistently started with a minimum of three and a maximum of five hydrogen bonds and remained stable with an average of three hydrogen bonds after 100 ns. Figure 3a and b visually presents the numbers and distances of these hydrogen bonds. In addition, the data in Figure 3C show that the minimum distances ranging between 0.15–0.25 nm for MMP-9 started to increase after 20 ns; for HAase, the initial range of 0.15–0.25 nm decreased after 50 ns and stabilized. For NF-κB, the minimum distance remained constant between 0.15–0.23 nm. These findings indicate that the 4′-Hydroxyflavone_MMP-9 complex exhibits weak and unstable hydrogen bonds, whereas the Isoquercitrin_HAase and Primulaverin_NF-κB complexes have strong and stable hydrogen bonds.

Molecular dynamics simulations are a critical tool in understanding the structural dynamics of protein–ligand complexes and their interactions with solvent. In this study, solvent accessible surface areas (SASA) and radii of gyration (Rg) were investigated. Figure 3c and d shows how these properties vary. In particular, the 4′-Hydroxyflavone_MMP-9 complex exhibited relatively increased fluctuations up to 45 ns, while exhibiting a more constant SASA value in the range 45–100 ns. This indicates that the complex has structurally transitioned from a more dynamic phase to a stable phase. In addition, the Rg plot presented for this complex showed high values at the beginning of the simulation but flattened over time to a more stable structure. On the other hand, the Isoquercitrin_HAase and Primulaverine_NF-κB complexes maintained their generally stable structures without any noticeable variation in both SASA and Rg values.

3.7 | Multivariate analysis

For a clearer understanding of the variation in biomolecules across eight samples, a heatmap was generated. In the plot presented in Figure 4, blue and red colors represent concentrations lower and higher than the mean, respectively. It is worth noting that the samples are divided into two main groups: rhizomes versus aerial parts. Within each group, the EA extract notably differs from the other extracts. Upon scrutinizing the biomolecule levels across all samples, we notice a higher concentration of protocatechuic acid (pv7), isorhamnetin 3,7-*O*-dihexoside (pv37) and nepetin 7-*O*-deoxyhexosyl-hexoside (pv44) in the aerial part water extract. Similarly, quercetin 3,7-*O*-dihexoside (pv35), flavone 4′-*O*-dihexoside (pv61), 5-hydroxy-4′-methoxyflavone 7-*O*-hexoside (pv62), isorhamnetin 3-*O*-dihexoside

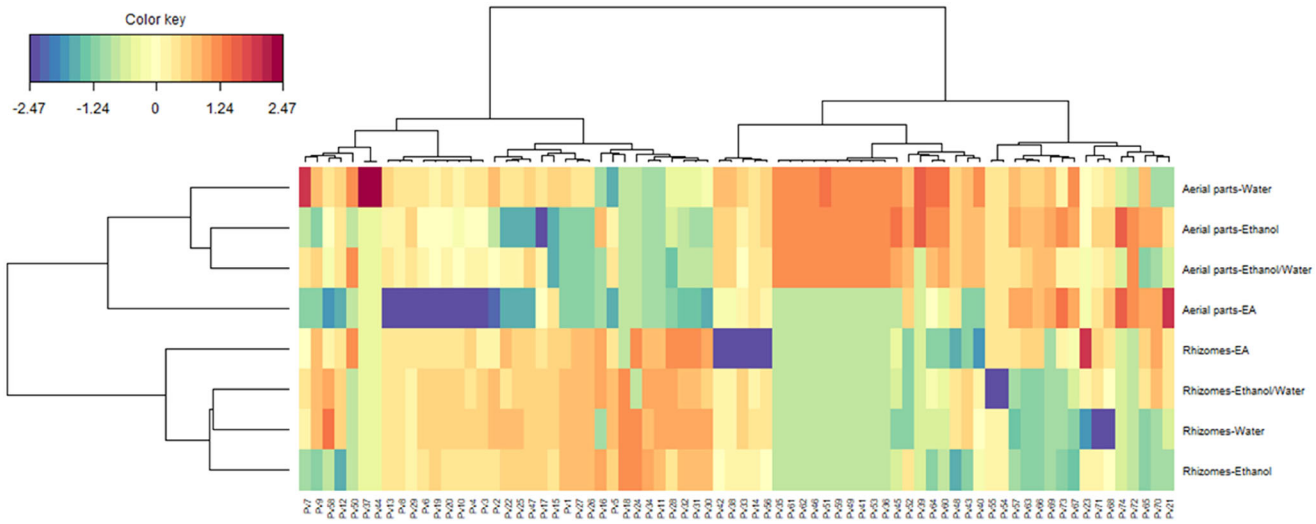

FIGURE 4 Global overview of the biomolecule's contrasts among *P. vulgaris* samples (blue color: low content; red color: high content).

(pv46), isorhamnetin 3-*O*-pentosylhexoside (pv51), 3′-hydroxyflavone 4′-*O*-dihexoside (pv59), nepetin 7-*O*-pentosylhexoside (pv49), 3′-hydroxy-4′-methoxyflavone 7-*O*-dihexoside (pv41), isorhamnetin 3-*O*-rutinoside (pv53), isorhamnetin 3-*O*-dihexoside-7-*O*-hexoside (pv36), luteolin (pv64), 3′-hydroxyflavone 4′-*O*-hexoside (pv60) were found to be more abundant in the water, ethanol, ethanol–water extracts of aerial parts. Finally, compared to the extracts high amounts of gallocatechin/epigallocatechin (pv34), syringic acid (pv11), roseoside (pv28), primulaverin/primverin (pv32), primulaverin/primverin (pv31), gaultherin (pv30) were found in the rhizome's extracts.

After conducting one-way ANOVA analysis, the data underwent principal component analysis (PCA) to uncover significant information that might have been overlooked with a univariate analysis approach. Initially, we selected the components that captured most of the variation in data. Subsequently, the first three principal components, collectively representing nearly 87% of the variance, were chosen. Specifically, these retained components explained 43%, 32%, and 12% of the total variability, respectively (Figure 5a).

Next, we investigated the relationship between biological activities and each principal component, as depicted in Figure 5b. It became evident that the first principal component accounted for variation in antioxidant properties (CUPRAC and FRAP), metal chelating, and inhibition against AChE and tyrosinase. The second component illustrated fluctuations in DPPH, ABTS and inhibition against amylase, while the third component referred to variation in inhibition toward glucosidase.

Figure 5a presented the distribution of the eight samples on a scatter plot, utilizing PC1 versus PC2, PC1 versus PC3, and PC2 versus PC3, respectively. Overall, a high variability was observed among the samples. However, there does not appear to be a distinct grouping of extracts. Thus, to obtain a clearer understanding of the shared characteristics among the studied samples, a Clustered Image Map based on the results of PCA and focusing on the first three retained principal components, was generated. As depicted in Figure 6, the samples were classified into three clusters. The first cluster (comprising aerial parts—water, aerial parts—ethanol/water, and rhizome—water) exhibited overall lower biological properties. In contrast, the third cluster (rhizome—ethanol, rhizome—EA, rhizome—ethanol/water), brought together extracts with notable biological activities. Finally, the Pearson's correlation analysis revealed the significant involvement of several molecules in the studied biological activities (Figure 7).

3.8 | The effect of *Primula vulgaris* on the inhibition of AGE

Inhibition of advanced glycation end products (AGEs), obtained through inflammation or food, are the result of an irreversible reaction between the amino groups of proteins and the reactive sugars through caramelized products (Chen et al., 2022; Fang et al., 2022; Meertens et al., 2016). Many studies in the literature have shown that AGE accumulation induces molecular mechanisms that cause the development of many skin problems, especially inflammatory skin problems, and skin aging, by physiologically affecting different skin layers (Chen et al., 2022; Fang et al., 2022; Gkogkolou & Böhm, 2012). The basis of this study is to illuminate the role of *Primula vulgaris* in the treatment of inflammatory skin diseases at the molecular level. In this context, according to the results presented in Figure 8, it was found that the extracts obtained from both rhizomes and aerial parts of the *Primula vulgaris* plant inhibit the formation of AGEs. The extracts with the highest inhibition activity were listed as rhizome—EtOH/water (93.7 %) > rhizome—EA (85.11 %) > aerial parts—EtOH/water (83.07 %) > rhizome—water (78.91 %) > aerial parts—EA (75.28 %) > aerial parts—EtOH (74.16 %) > rhizome parts—EtOH (70.28 %) > aerial parts—water (57.05%), respectively (Figure 8a). The inhibition activity of Quercetin in 1 mg/mL used as a positive control was determined by 95.64% (Figure 8b). As a result of the analyses, it was observed that similar results were obtained compared to the EtOH/water extract obtained from the rhizomes

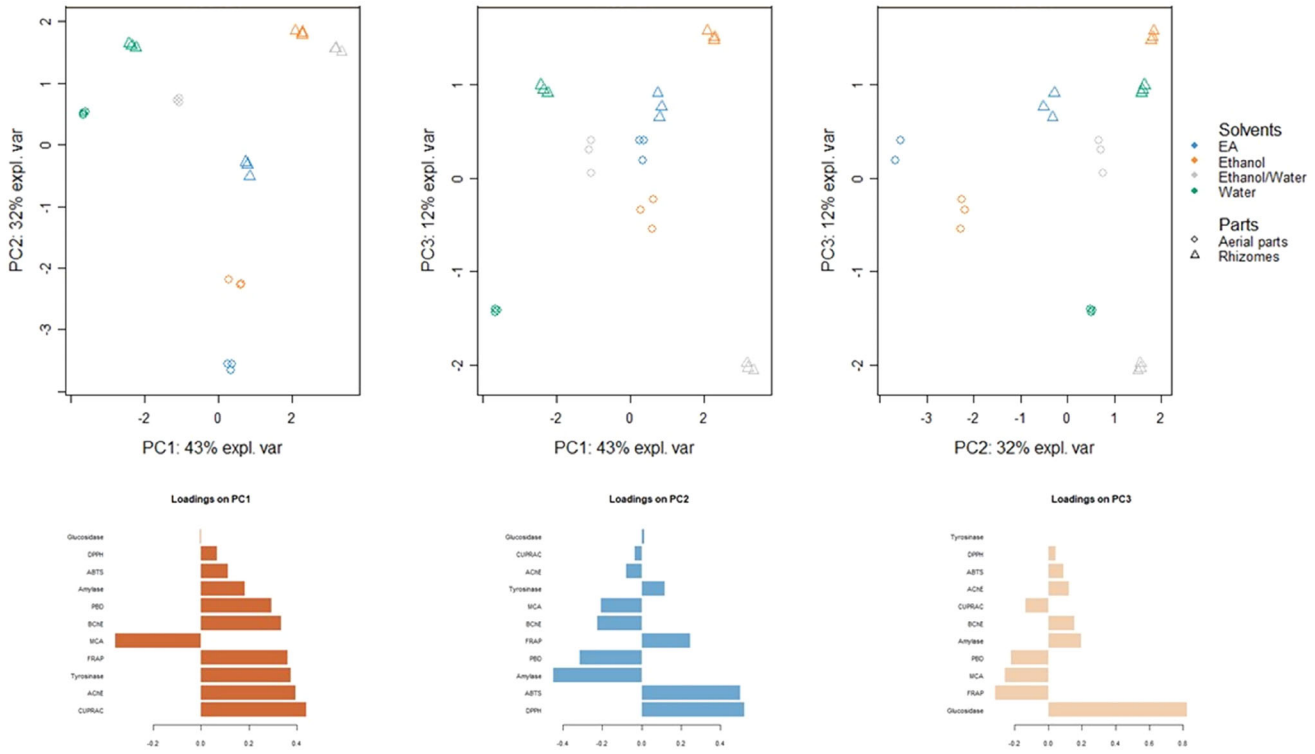

FIGURE 5 Exploratory multivariate analysis on biological activities. (a) Scatter plots of PCA. (b) Contribution of biological activities on the first three components of PCA.

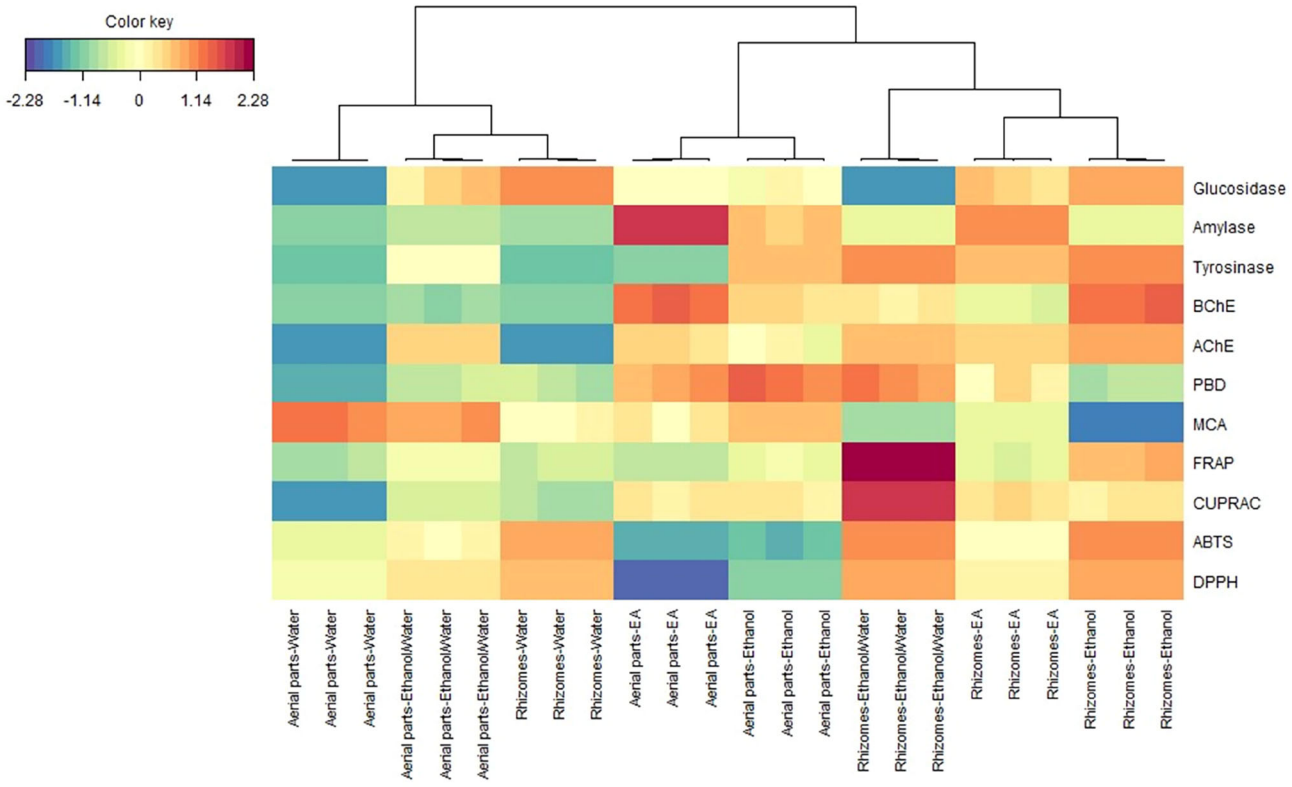

FIGURE 6 Clustered Image Map on biological activities dataset (blue color: low bioactivity; red color: high bioactivity).

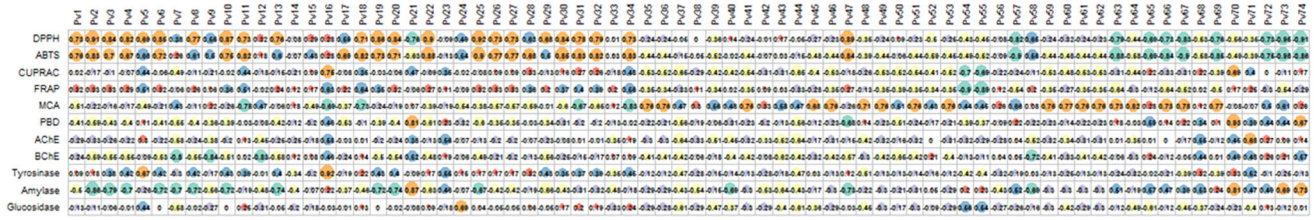

FIGURE 7 Relationship between biomolecules and biological activities of *P. vulgaris* samples.

FIGURE 8 AGEs inhibition potential of eight different extracts obtained from the aerial parts and rhizomes of *Primula vulgaris*. The % of AGE inhibition potential of eight different extracts at 1 mg/mL obtained from *Primula vulgaris* was presented in Figure 8a. The AGE inhibition value of Quercetin, which was selected as a positive control, at increasing concentration was shown in Figure 8b. Statistical analyses were performed using the one-way ANOVA tab of the GraphPad Prism 10 software program. While ns was used for samples that showed a nonsignificant difference with the compared group, * was used for the smallest significant value $p \leq .05$. ** was symbolizes $p \leq .01$, while **** was used for $p \leq .0001$.

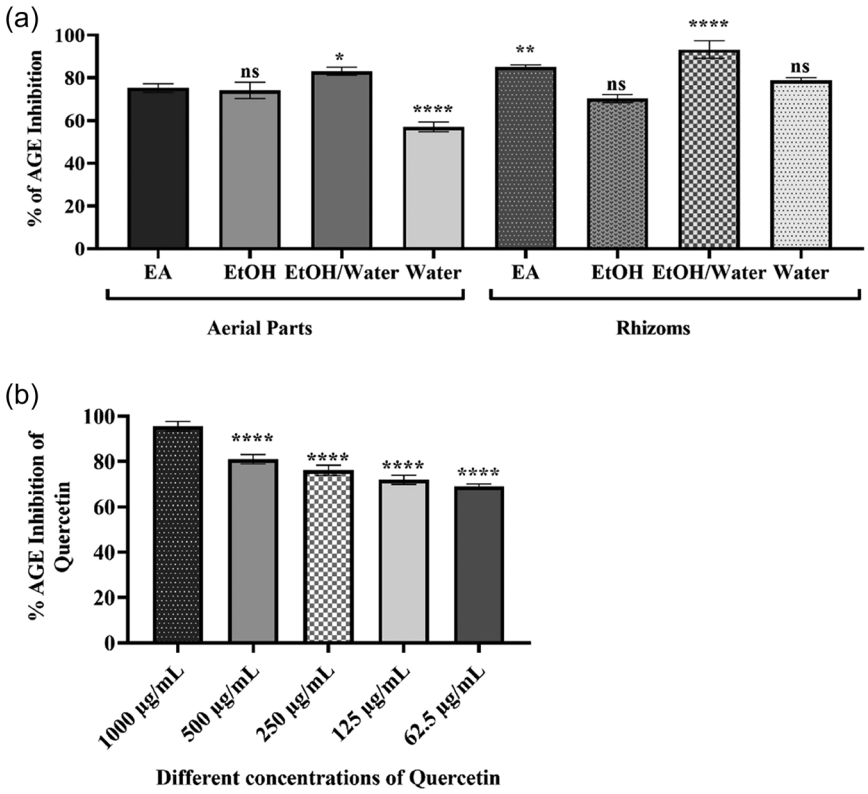

of the *P. vulgaris* in 1 mg/mL concentration. On the other hand, the results are similar to the total phenolic and flavonoid content tests of the plant. According to the phytochemical analysis, the plant *P. vulgaris* is rich in biomolecules, as shown in Table 2. It has been revealed that the various extracts obtained from different parts of *P. vulgaris*, such as *P. auriculata*, known to have an AGEs inhibition activity in the literature, have high antioxidants and phytochemical compositions (Kurt-Celep et al., 2022). In particular, the biocomponents such as p-coumaric acid, chlorogenic acid, caffeic acid, gaultherin, salicylic acid, quercetin, isoquercitrin, hyperoside, which are possessed by *P. vulgaris* extracts, have prevented the formation of AGEs due to their high antioxidant potential (Gkogkolou & Böhm, 2012; Michel et al., 2022; Shen et al., 2019). In addition, these compounds in the extracts have also exhibited a natural anti-inflammatory effect (Alam et al., 2024; Turan et al., 2023). In this case, *P. vulgaris* with high antioxidant potential can be a candidate to become a natural AGEs inhibitory.

3.9 | Determination of nontoxic concentration and cytoprotective potential of *Primula vulgaris*

Thanks to the various phytochemical content of the tested extracts presented in Table 2, it has been shown that the plant may have high anti-inflammatory properties and ROS scavenging activity. In the light of this content analysis, human dermal fibroblast cells (HDF), which were induced by lipopolysaccharide, were selected as model cells for the in vitro study. Our aim is to explain the role of *P. vulgaris* in the treatment of anti-inflammatory skin diseases at the molecular level. First of all, the WST-1 test was performed to determine the noncytotoxic concentration of eight different extracts obtained from the *P. vulgaris* to be applied to HDF cells. After the extract was treated with cells for 48 h, the method described in "Cell Culture and Viability" part was applied. At the end of the 48th hour, the viability of the untreated HDF control cell was accepted by 100% for each extract. In the highest concentrations of EA, EtOH, EtOH/water, and water extract obtained

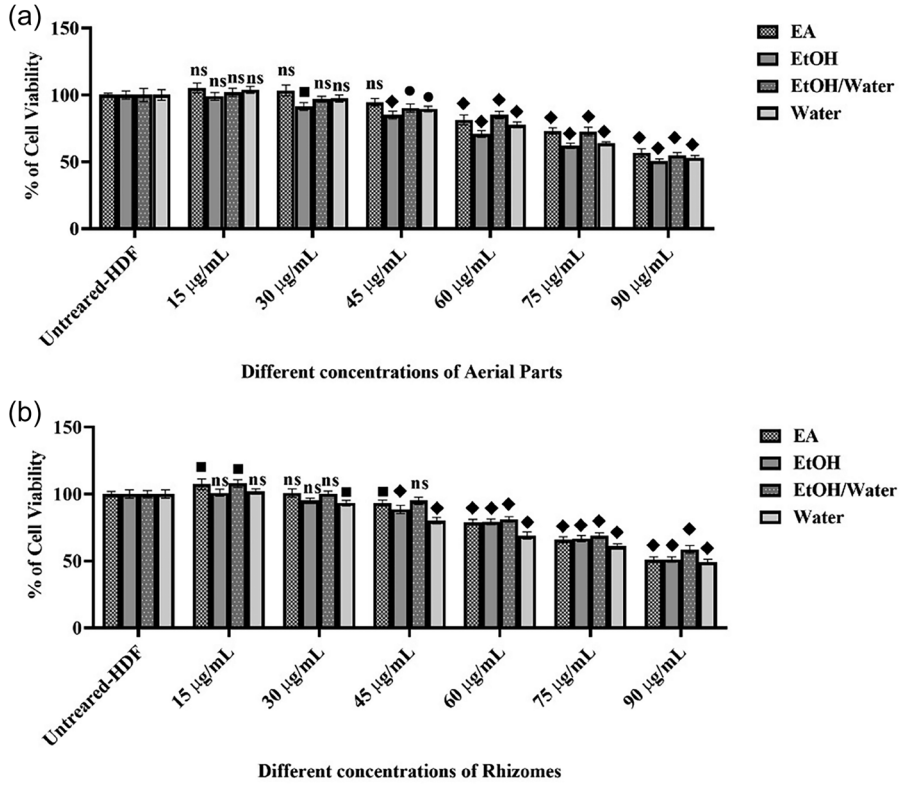

FIGURE 9 Determination of the nontoxic concentration of extracts obtained from *Primula vulgaris* on the HDF cell line and their effects on cell viability using WST-1 The effects of EA, EtOH, EtOH/water, and water extracts, respectively, obtained from the aerial parts of *Primula vulgaris*, on the viability of HDF cells at increasing concentrations are shown in Figure 9a. In Figure 9b, the effect of extracts obtained from the rhizomes of *Primula vulgaris* on cell viability is presented. Extracts in quantitative analyses were applied to HDF cells in increasing concentrations for 48 h. Statistical analysis was performed by selecting multiple comparisons in the two-way ANOVA tab of the GraphPad Prism 10 software program. ns was used to show similar results to the control group to which it was compared and indicates that there is no significant difference. While ■ was used for $p \leq .01$, ● was used for $p \leq .001$. The shape ♦ corresponds to the value $p \leq .0001$.

from the aerial part of *P. vulgaris* to HDF cells, cell viability was detected by 56.74%, 50.49%, 54.93%, and 52.93% presented in Figure 9A. The values obtained from the rhizomes of *P. vulgaris* in the same experimental setup and concentration are 50.93%, 51.06%, 58.7%, and 49.07%, respectively (in Figure 9B). According to the findings presented in Figure 9, 75 µg/mL is the common working concentration in all extracts with a cell vitality rate of not less than 50% (Kurt-Celep et al., 2022). However, the elevated concentration of the extract causes the cells to exhibit cytostatic actions. Studies in the literature have observed that many cancer cell lines can cause cell death due to the presence of saponin chemicals found in different species of *Primula* (Alam et al., 2024; Bączek et al., 2017; Elekofehinti et al., 2021; Kurt-Celep et al., 2022). Saponins are known as natural detergent derivatives and polar glycosides containing a sugar group of triterpene/steroid aglycone (Kurt-Celep et al., 2022; Wisetkomolmat et al., 2020). The most remarkable features are that it has anticarcinogenic activity, especially in cancer cells by providing induction of apoptosis through cytotoxicity (Elekofehinti et al., 2021). In addition to the anticancer effect of *Primula* species, another study conducted on fibroblast cells found that they have a cytostatic effect on cells depending on the concentration. In the same study, it was observed that *P. vulgaris* has a cytoprotective effect at a nontoxic concentration in H_2O_2-treated fibroblast cells (Tugce Ozkan et al., 2017). In the phytochemical content analysis of *P. vulgaris* presented in Table 2, aglycones of isorhamnetin numbered 36, 37, 42, 46, 50, 51, 53, 56, and 72 were found in different extracts. A study conducted with hepatocyte cells has shown that a medicinal plant containing aglycone isorhamnetin can be used in the treatment of cancer by creating a cytotoxic effect in cells (Teng et al., 2006). Based on our results, which are compatible with the information in the literature, it has been shown that the various phytocompounds contained in *P. vulgaris* can have antitumor and anticancer effects in cancer cells, and in addition have a cytoprotective effect in inflammation or wound healing fibroblast cells.

3.10 | Elimination of mitochondrial oxidation with *Primula vulgaris*

Following the 10 µg/mL of LPS applied to HDF cells, the DCFDA method was performed to illuminate the role of *P. vulgaris* in reducing the increasing oxidation in the cells. Following the administration of eight different extracts obtained from *P. vulgaris* to the HDF + LPS cell group for 48 h, the changing ROS level in these cells were detected compared to the untreated-HDF group (Figure 10). Since the ROS level

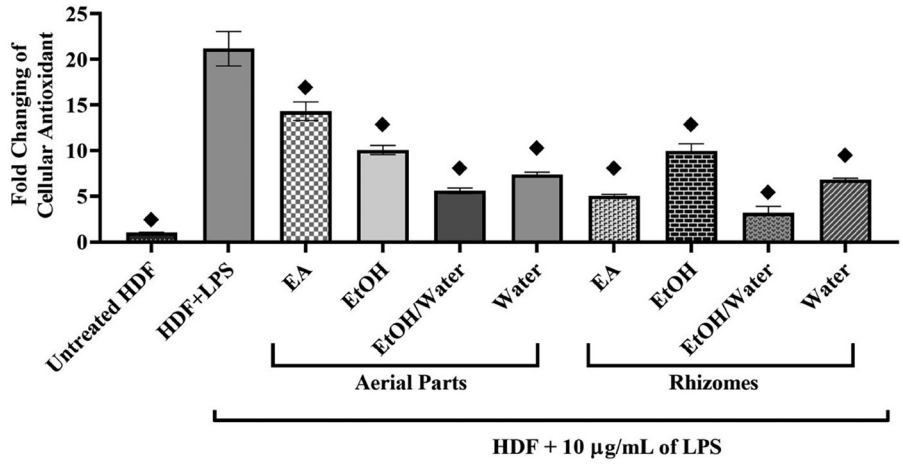

FIGURE 10 Determination of the ROS scavenging effect of *Primula vulgaris* on LPS-induced HDF cells with DCFDA. The ROS scavenging activity of eight different *Primula vulgaris* extracts at a concentration of 75 µg/mL applied to the LPS-induced HDF cell group for 48 h and fold change was presented in Figure 10. In the results analyzed comparatively with the HDF + LPS cell group, the multiple comparisons option of the one-way ANOVA tab in the GraphPad Prism 10 software program was used and the value $p \leq .0001$ was expressed with the ♦.

in untreated-HDF cells was accepted onefold, the ROS formation was detected 21.18-fold in HDF+LPS cells. When HDF + LPS cells and the extracts obtained from the aerial parts applied to this group of cells were compared, the ROS level was decreased by 1.5 times for EA, 2.10 times for EtOH, 3.79 times for EtOH/water, and 2.87 times for Water (Figure 10). It was found that the ROS level decreased by 4.21 times, 2.13 times, 6.68 times, and 3.09 times, respectively, in the extracts obtained from the rhizomes, where a similar comparison was made. As a result of the statistical analyses, the highest cellular ROS scavenging activity was listed as rhizome—EtOH/water > rhizome—EA > aerial parts— EtOH/water > rhizome—water > aerial parts—water > rhizome—EtOH > aerial parts—EtOH > aerial parts—EA (Figure 10, ♦ means $p \leq .0001$). LPS is an endotoxin found in the outer membrane of Gram-negative bacteria and is a proinflammatory agent (Guarneri et al., 2021). Various immune reactions can occur in cells treated with LPS, such as inflammation, antibody development, increased cytokine release, and even septic shock (Fock & Parnova, 2021; Guarneri et al., 2021). On the other hand, it is known that there is a cross-talk between LPS and an increase in the level of ROS in cells (Fock & Parnova, 2021; Sul & Ra, 2021). Many studies have shown that both cytosol and mitochondrial ROS accumulation leads to an increase in NFKB via LPS and that the inflammation pathway is triggered due to a shift in ROS /Antioxidant balance in cells (Fock & Parnova, 2021; Sul & Ra, 2021). The amount of mitochondrial ROS was measured with fluorogenic dye in experimental sets in which many animal models were applied, and it was observed that the production of superoxide in mitochondria increased with the exposure of cells to LPS (Fock & Parnova, 2021; Shen et al., 2019). On the other hand, it is essential to increase the antioxidant level in the cells in order to eliminate ROS. As is known, plants are natural sources of antioxidants and play an important role in restoring the ROS/Antioxidant balance thanks to various phytochemicals (Akbari et al., 2022). Plants provide nonenzymatic antioxidant defense thanks to their low cytotoxic effect, various molecules such as flavonoids, alkaloids, and glycosides (Akbari et al., 2022; Dumanović et al., 2021). *P. vulgaris* is one of these plants. It has been shown that ROS can have a scavenging effect thanks to both the rich phytochemical compounds and its high antioxidant capacity presented in Tables 1 and 2. Figure 10, which supports this hypothesis and covers the DCFDA results in which the mitochondrial ROS level was measured, supports our theory. It was observed that the amount of ROS decreased significantly after applying extracts obtained from both the rhizomes and aerial part of *Primula vulgaris* to HDF + LPS group cells (Figure 10, ♦ means $p \leq .0001$). It can be said that this condition is due to compounds such as coumaric acid, chlorogenic acid, caffeic acid, primulaverin/primverin, quercetin, hyperoside, kaempferol, and quercitrin, which *P. vulgaris* has (Alam et al., 2024; Dumanović et al., 2021; Kurt-Celep et al., 2022). In a large number of studies were shown that different *Primula* species have antioxidant properties due to their chemical profile (Alam et al., 2024; Bączek et al., 2017; Kurt-Celep et al., 2022). In addition to this information, it has been added to the literature that the mitochondrial ROS level induced in HDF cells by LPS under in vitro conditions has been eliminated by the tested extracts.

3.11 | The effect of *P. vulgaris* on the molecular pathway of inflammation

Western blot technique was used for determining the level of proteins that play a role in the inflammation process. The levels of target proteins described in Western blot section were presented in Figure 11. In this context, the level of each protein in untreated-HDF cell was proportional to beta-actin and the change was calculated as 1 time. The value of phospho-NFKB, Rage, AP-1, IL-6, IL-17, and TNF-alpha target proteins has been detected compared to this change (Figure 11, ♦ Means $p \leq .0001$). The ImageJ program was used for the quantitative analysis of the western image presented in Figure 11a and the

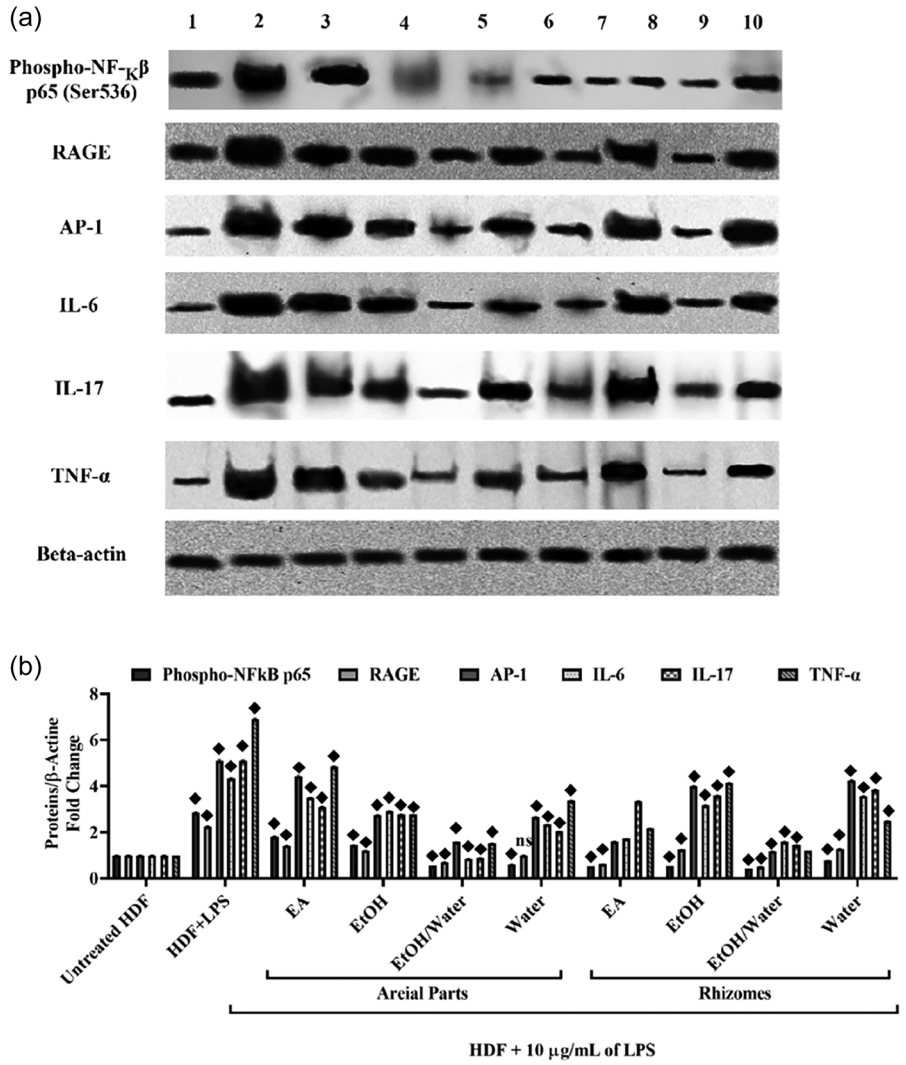

FIGURE 11 Effect of *Primula vulgaris* on the inflammation pathway in LPS induced-HDF cells. Western blotting was performed to detect altered protein levels after *Primula vulgaris* was applied to LPS + HDF cells (in Figure11a). Beta-actin housekeeping protein was used to show that protein amounts were loaded equally. While band intensities were measured with the Gel tab of the ImageJ program, the multiple comparisons option of the one-way ANOVA tab of the GraphPad Prism 10 software program was used for statistical analysis (in Figure11b). As a result of the analyses made by comparing the band density of untreated-HDF cells, nonsignificant results were shown with ns, while the ♦ was used for $p \leq .0001$ value. 1: untreated-HDF, 2: HDF+LPS, 3: HDF+LPS + EA aerial parts, 4: HDF+LPS + EtOH aerial parts, 5: HDF+LPS + EtOH/water aerial parts, 6: HDF+LPS + water aerial parts, 7: HDF+LPS + EA rhizomes, 8: HDF+LPS + EtOH rhizomes, 9: HDF+LPS + EtOH/water rhizomes, 10: HDF+LPS + water rhizomes.

results were included in Figure 11b. As a result of the analysis, it was found that the levels of phospho-NFKB, RAGE, AP-1, IL-6, IL-17, and TNF-alpha target proteins increased 2.85-fold, 2.25-fold, 5.10-fold, 4.34-fold, 5.23-fold, and 6.91-fold in HDF + LPS cells compared to untreated HDF cells, respectively (Figure 11b, $p \leq .0001$). It was observed that phospho-NFKB, RAGE, AP-1, IL-6, IL-17, and TNF-alpha levels decreased by 1.82, 1.42, 4.43, 3.50, 3.10, and 4.85 times, respectively, when EA obtained from aerial parts was applied to the HDF + LPS cell group. In a similar comparison made after the application of EtOH aerial parts, it was observed that these values decreased by 1.45, 1.22, 2.74, 2.92, 2.77, and 2.79 times, respectively. After applying EtOH/water extract obtained from aerial parts to HDF + LPS cells, phospho-NFKB level decreased to 0.56, RAGE to 0.71, AP-1 to 1.58, IL-6 levels to 0.85, IL-17 to 0.89, and TNF-alpha level decreased to 1.53. In a similar comparison made after the application of water extract of aerial parts, it was analyzed that these values were 0.61 times, 1 time, 2.66 times, 2.35 times, 2.04 times, and 3.38 times, respectively. On the other hand, when EA obtained from rhizomes was applied to the HDF + LPS cell group, it was observed that phospho-NFKB, RAGE, AP-1, IL-6, IL-17 and TNF-alpha levels decreased by 0.53 times, 0.62 times, 1.6 times, 1.72 times, 3.35 times, and 2.17 times, respectively. Phospho-NFKB level was calculated by 0.55-fold, RAGE level by 1.26-fold, AP-1 level by 4-fold, IL-6 level by 3.17-fold, IL-17 level by 3.59-fold, and TNF-alpha level by 4.14-fold in rhizomes EtOH-treated HDF + LPS cells. In similar comparison after rhizomes—EtOH/water application, it was found that these values decreased to 0.44 times,

0.51 times, 1.59 times, 1.45 times, and 1.21 times, respectively. Finally, after applying the water extract obtained from the rhizomes to the HDF + LPS cell group, phospho-NFKB, RAGE, AP-1, IL-6, IL-17, and TNF-alpha protein levels were found by 0.77-fold, 1.28-fold, 4.26-fold, 3.56-fold, 3.84-fold, and 2.49-fold (in Figure 11). As is known, a number of inflammatory pathways involving the signaling of molecules such as ROS-induced NFKB, RAGE, AP-1, IL-6, IL-17, and TNF alpha are activated as a result of treating cells with LPS, which is an extracellular component of Gram-negative bacteria and is commercially available (Guarneri et al., 2021; Hsu & Wen, 2002; Nguyen et al., 2021; Park et al., 2015). NFKB, which is a transcription factor, is complex with the inhibitor of Kappa B (Iκb) under normal conditions and thus inactive form (Nennig & Schank, 2017; Singh & Singh, 2020). In order for NFKB to be activated, the proteosomal degradation of the IKB must take place and the NFKB must be phosphorylated and then translocated into the nucleus (Serasanambati & Chilakapati, 2016; Singh & Singh, 2020). IkB-kinase (IKK) complex is stimulated by LPS and triggered to phosphorylate IKB, which causes proteasomal degradation of IKB, and NFKB is translocated to the nucleus, where it passes into the active form and initiates the inflammation process (Nguyen et al., 2021). Phospho-NFKB, which is active in the nucleus, induces the release of inflammatory cytokines such as IL-6, IL-17, and TNF alpha by stimulating activator protein-1 (AP-1) (Serasanambati & Chilakapati, 2016; Singh & Singh, 2020; Subedi et al., 2019; Wu & Zhou, 2010). The AP-1 protein is a transcription factor that plays a role in inflammation, cancer development, cell survival and cell migration (Bhosale et al., 2022). In recent studies, inhibitors targeting NFKB and AP-1 have been new approaches to treatment (Bhosale et al., 2022; Serasanambati & Chilakapati, 2016). On the other hand, it is known that RAGE is an AGEs receptor, and it has crosstalk with active NFKB in the inflammation process (Guarneri et al., 2021). Studies has been shown the level of RAGE increases in cells treated with LPS and plays a role in inflammation (Guarneri et al., 2021). NFKB was phosphorous and activated after the application of 10 µg/mL concentration of LPS to HDF cells in parallel with the literature and the results of Figure 11. RAGE, AP-1, IL-6, IL-17, and TNF-alpha molecules are induced by active NFKB and they play an important role in initiating the inflammation process. While the level of these transcription factors and cytokines increased with LPS treatment, it was found that the levels of the tested extracts decreased with the level of all target proteins. A549, HepG2, MCF-7, and PC-3 cancer cell lines were used in a *P. vulgaris* study, and it was stated that the plant has both an anti-cancer effect and an antioxidant effect, and these properties are due to phenolic compounds and flavonoids (Demir et al., 2019). Other studies that corroborate our findings have also examined the anti-inflammatory properties of various *Primula* species from a molecular perspective. Flavonoids, particularly those from *Primula* species, may be precursor compounds in inflammation suppression. These results indicate that *P. vulgaris* has an anti-inflammatory effect and can be used in the treatment of inflammatory skin diseases (Alam et al., 2024; Bączek et al., 2017; Kurt-Celep et al., 2022).

3.12 | Modulation of enzymes and MMPs involved in the regulation of ECM stabilization by *Primula vulgaris*

The results of analyzing the effects of eight different extracts obtained from both aerial parts and rhizomes of *P. vulgaris* on the enzymes collagenase, elastase, and hyaluronidase, respectively, which are known to play a role in ECM regulation, are presented in Figure 12. On the other hand, the varying levels of MMP-2 and MMP-9 in LPS-induced HDF cells where *Primula vulgaris* was administered for 48 h are presented in Figure 13. According to the results obtained in Figure 12, the inhibition values of EA, EtOH, EtOH/water, and water extracts obtained from the aerial and rhizome parts of *P. vulgaris* are 71.09%, 79.83%, 86.41%, 81.17%, 87.94%, 80.065, 91.68%, and 82.26%, respectively. The inhibition value of 250 µg/mL of EGCG used as a positive control for collagenase inhibition was calculated as 95.91% (in Figure 12a). In Figure 12b, EA extract obtained from the aerial part had elastase inhibition of 68.23%, EtOH of 73.01%, EtOH/water of 83.95%, and water extract of 80.84%. In the rhizome extract, where similar results were obtained, these values were calculated as 86.08%, 77.19%, 92.07%, and 81.14%, respectively, while this value was determined as 96.93% for the positive control EGCG. Figure 12c shows the quantitative results of the anti-hyarolunidase activity of the tested extracts. For anti-hyarolunidase activity, 250 µg/mL of tannic acid was chosen as a positive control (Barak et al., 2023; Barak et al., 2022; Ersoy et al., 2019). According to the results obtained, the highest inhibition activity was listed as rhizomes—EtOH/water (90.05%) > rhizomes—EA (87.04 %) > aerial parts—EtOH/water (84.27 %) > rhizomes—water (82.33 %) > aerial parts—water (80.73 %) > rhizomes—EtOH (75.29 %) > aerial parts—EtOH (74.06 %) > aerial parts—EA (65.93%). Tannic acid inhibition was detected at 94.28%. In the zymography results, where MMP-2 and MMP-9 inhibitions were evaluated, MMP biosynthesis was reduced following the 75 µg/mL of aerial parts and rhizome extracts applied to HDF + LPS cells for 48 h (Figure 13a. In the quantitative analysis, the band intensities of HDF + LPS cells in both MMP-2 and MMP-9 were considered 100% (in Figure 13b and c). In this context, after the application of EA, EtOH, EtOH/water, and water extracts obtained from the aerial parts to HDF + LPS cells, MMP-2 activity was detected at a rate of 66.99%, 51.28%, 25.08%, and 35.06%, respectively. In rhizomes extracts, where a similar comparison was made, these values were determined as 19.55%, 43.58%, 23.07%, and 34.40% (Figure 13b). On the other hand, in MMP-9 quantitative analysis, 73.16% for aerial parts—EA, 56.26% for aerial parts—EtOH, 13.96% for aerial part—EtOH/water, 33.38% for aerial part-water, 24.37% for rhizomes—EA, 47.33% for rhizomes—EtOH, 12.05% for rhizomes—EtOH/water, and 33.28% for rhizomes—water were found and present in Figure 13c. In untreated-HDF cell groups, MMP-2 activity was detected at a rate of 17.46%, while MMP-9 activity was observed at a rate of 11.68%. ECM, which is called the outermost part of the skin, consists of elastin, fibrinogen, hyaluronic acid and many structural proteins, mainly collagen (Jiratchayamaethasakul

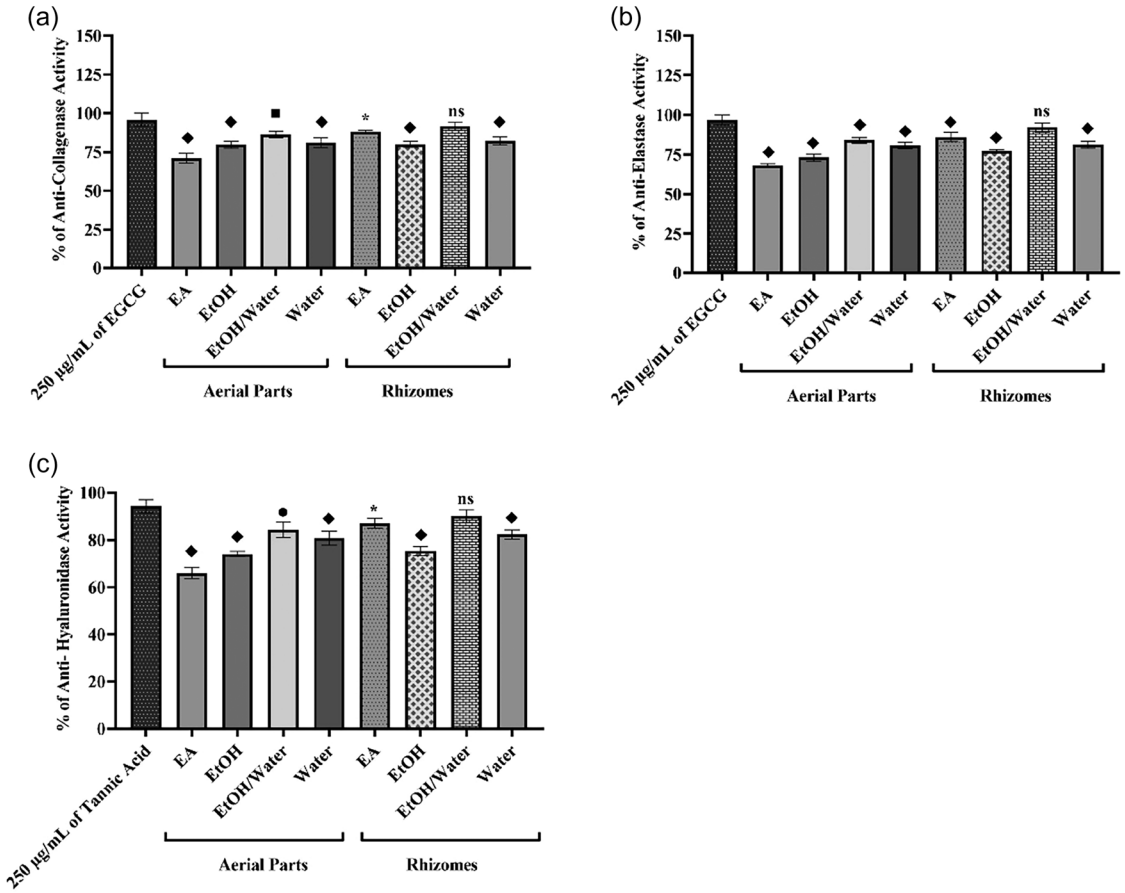

FIGURE 12 Effect of eight different extracts obtained from *Primula vulgaris* on skin enzymes. The inhibitory potential of eight different extracts obtained from *Primula vulgaris* on collagenase (in Figure 12a), elastase (in Figure 12b), and hyaluronidase (in Figure 12c) enzymes, respectively, which are involved in the regulation of the skin barrier, has been demonstrated. While EGCG was used as a positive control in collagenase and elastase enzyme experiments, tannic acid was used as a positive control in hyaluronidase activity. Statistical analyses were performed with the multiple comparisons option of the one-way ANOVA tab of the GraphPad Prism 10 software program. ns was used for nonsignificant results, * was used for $p \leq .05$, ● was used for $p \leq .001$, and ♦ was used for $p \leq 0.0001$.

et al., 2020; Sun, 2021). Collagen is one of the most abundant components among extracellular matrix proteins and is one of the main components that strengthen the connective tissue. Thanks to collagen, ECM is more resistant to injuries, impacts and inflammation (Sun, 2021). Elastin is a fibril network consisting of elastic fibrils tightly connected to collagen fibrils. According to the elastin, the return to its original shapes after the jam or stretch of the ECM provides flexibility to the skin (Sun, 2021). Hyaluronic acid or hyaluronan (HA) is a glucose-based polymer found in both the dermis and epidermis of the skin (Bayer, 2020). HA has the ability to retain water and thus helps to moisturize the skin while at the same time supporting the skin barrier (Bayer, 2020; Sun, 2021). The collagenase and elastase are responsible for the breakdown of collagen and elastin fibrils, respectively (Bayer, 2020). In cases where the effectiveness of ROS increases, such as aging or inflammation, the level of hyaluronidase enzyme responsible for the breakdown of HA increases in the skin (Bayer, 2020). Increased levels of the collagenase, elastase, and hyaluronidase cause the skin to age and become susceptible to microorganism invasion and inflammation (Lu et al., 2011). On the other hand, another family of enzymes that help in maintaining ECM stabilization is MMPs (Lu et al., 2011). While the secretion of MMPs at the basal level plays an important role in the regeneration of broken intercellular fibrils and the repair of damaged tissue, the increase of their synthesis in the presence of various inflammatory agents such as LPS leads to loss of ECM integrity and deceleration of connective tissue (Loo et al., 2023; Ronsisvalle et al., 2020; Sun, 2021). The activation of MMPs is realized through the NFKB signal pathway (Loo et al., 2023). As a result of the separation of NFKB from IKB, MMPs are stimulated and their activation increases with possible translocation to the nucleus. In addition, as a result of AGE accumulation, the biosynthesis of MMPs increases, causing the development of various degenerations in the body, especially skin damage (Ronsisvalle et al., 2020). ECM homeostasis or restore the lost ECM integrity, the presence of various plant extracts, which are a natural source of flavones and flavonols, especially in the content of dermocosmetic products, has become a new strategy. Thus, medical plants are the main actors in the treatment of various skin diseases, especially skin aging, eczema and psoriasis (Chaiyana et al., 2020; Ronsisvalle et al., 2020). As a result of the increase of NFKB and TNF-alpha

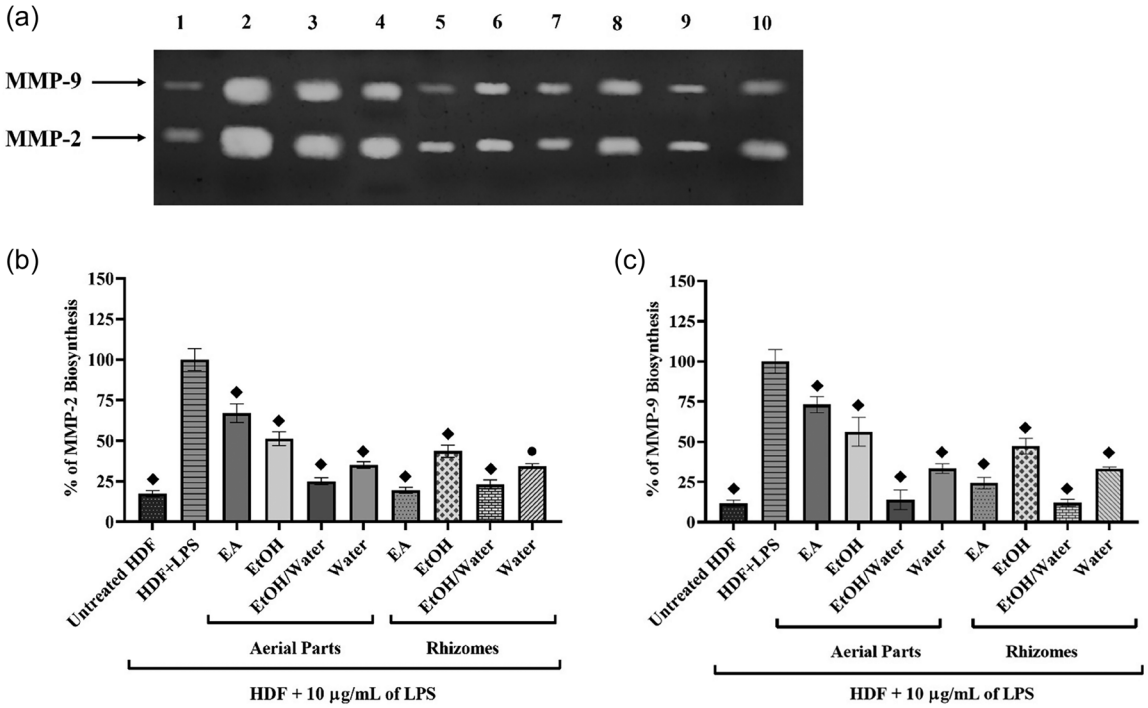

FIGURE 13 The role of *Primula vulgaris* in MMP regulation in HDF cells with impaired LPS-mediated ECM integrity. The effect of extracts obtained from *Primula vulgaris* on gelatinase MMPs involved in ECM regulation in HDF + LPS cells was demonstrated by zymography. MMP-2 and MMP-9 lytic bands are presented in Figure 13a. Figure 13b and Figure 13c show the band intensities for which quantitative results were obtained with the ImageJ Gel program. The multiple comparisons option of the one-way ANOVA tab in the GraphPad Prism 10 software program was used in the statistical analysis. While the ● is used for the value $p \leq .001$, the $p \leq .0001$ value is expressed with the symbol ◆. 1: untreated-HDF, 2: HDF+LPS, 3: HDF+LPS + EA aerial parts, 4: HDF+LPS + EtOH aerial parts, 5: HDF+LPS + EtOH/water aerial parts, 6: HDF+LPS + water aerial parts, 7: HDF+LPS + EA rhizomes, 8: HDF+LPS + EtOH rhizomes, 9: HDF+LPS + EtOH/water rhizomes, 10: HDF+LPS + water rhizomes.

in human dermal fibroblast cells treated with UV in literature, it was found that the activity of MMP-1, MMP-3, and collagenase increased in these cells. But in the same study, it was found that the ECM integrity that was lost was restored when a plant extract with a rich phytochemical content was applied to UV-induced cells (Loo et al., 2023). In a study with *P. vulgaris*, anti-collagenase and anti-elastase activity were observed in the butanol extract obtained from the root parts of the plant. It is pointed out in the same study that saponin and secondary metabolites in the root parts of *P. vulgaris* may be responsible for this inhibition activity (Kahraman et al., 2022). In another study, the extracts obtained from the aerial parts and the rhizomes parts of *P. auriculata* inhibited the ROS-guided overexpress MMP-2 and MMP-9 on the HT-29 colon cancer cell line and thus integrity of ECM is achieved and the metastatic feature may be reduced (Kurt-Celep et al., 2022). It has been determined in Figures 8–13 that the formation of IL-6, IL-17, AP-1, and TNF-α is prevented by suppressing the NFKB/RAGE signaling pathway thanks to AGE inhibition of *P. vulgaris*. In this way, the activities of collagenase, elastase, hyaluronidase, and gelatinase group MMPs (MMP-2 and MMP-9), which are stimulated by LPS and contribute to the deterioration of ECM integrity, were inhibited and skin damage was saved. In short, *P. vulgaris* indicated that the extracts obtained from both aerial parts and rhizomes can be used particularly in the treatment of inflammatory skin diseases and at the same time may be a candidate to become a natural MMP inhibitor.

4 | CONCLUSION

In conclusion, the extracts from rhizomes and aerial parts of *P. vulgaris* were rich in flavonoids. In addition to the antioxidant and enzyme inhibitory properties, the tested extracts were found to eliminate skin damage in HDF+LPS cells, where skin inflammation is mimicked by LPS treatment under in vitro conditions. At the same time, it has been observed that the ROS/antioxidant balance lost by LPS is regained with the extracts. The tested extracts were found to have no cytotoxic effect on HDF cells, while they were found to have anti-inflammatory properties. To obtain more insights, potential drug candidates were subjected to comprehensive molecular docking and molecular dynamics simulations targeting MMP-9, HAase, and NF-κB. Isoquercetin demonstrated superior efficacy, excelling in various metrics including radius of gyration, number of hydrogen bonds, and minimum distance measurements, according to both docking scores and dynamics evaluations. These results underscore isoquercetin's remarkable effectiveness, suggesting its significant potential as a therapeutic agent. While Pirimulaverin also demonstrated positive outcomes, it did not achieve the same level of performance as isoquercetin in the docking analysis or in molecular dynamics simulations. Thus, *P. vulgaris* can be a valuable raw material for the development of effective and safe functional applications, including pharmacetuicals, cosmeceuticals, and nutraceuticals. However, further studies are strongly recommended

to isolate the components and evaluate their individual biological and pharmacokinetic properties (bioavailability, etc).

ACKNOWLEDGMENTS

This study is financed by the European Union-NextGenerationEU, through the National Recovery and Resilience Plan of the Republic of Bulgaria, project No. BG-RRP-2.004-0004-C01.

CONFLICT OF INTEREST STATEMENT

The authors declare no conflicts of interest.

ETHICS STATEMENT

The paper don't any human and animal experiments.

ORCID

Gokhan Zengin https://orcid.org/0000-0001-6548-7823

REFERENCES

Acquaviva, A., Di Simone, S. C., Nilofar, Bouyahya, A., Zengin, G., Recinella, L., Leone, S., Brunetti, L., Uba, A. I., Guler, O., Balos, M., Cakilcioğlu, U., Menghini, L., Ferrante, C., Orlando, G., Libero, M. L., & Chiavaroli, A. (2023). Screening for chemical characterization and pharmacological properties of different extracts from *Nepeta italica*. *Plants*, *12*(15), 2785.

Agarwal, G., Carcache, P. J. B., Addo, E. M., & Kinghorn, A. D. (2020). Current status and contemporary approaches to the discovery of antitumor agents from higher plants. *Biotechnology Advances*, *38*, 107337.

Akbari, B., Baghaei-Yazdi, N., Bahmaie, M., & Mahdavi Abhari, F. (2022). The role of plant-derived natural antioxidants in reduction of oxidative stress. *BioFactors*, *48*(3), 611–633.

Alam, F., Din, K. M., Sarfraz, M., Qudoos, A., & Malik, S. (2024). Genus Primula and its role in phytomedicine; a systematic review. *Phytomedicine Plus*, *4*(1), 100510.

Arabi-Jeshvaghani, F., Javadi-Zarnaghi, F., & Ganjalikhany, M. R. (2023). Analysis of critical protein–protein interactions of SARS-CoV-2 capping and proofreading molecular machineries towards designing dual target inhibitory peptides. *Scientific Reports*, *13*(1), 350.

Avtanski, D., & Poretsky, L. (2018). Phyto-polyphenols as potential inhibitors of breast cancer metastasis. *Molecular Medicine*, *24*, 1–17.

Bączek, K., Przybył, J. L., Mirgos, M., Kosakowska, O., Szymborska-Sandhu, I., & Węglarz, Z. (2017). Phenolics in *Primula veris* L. and *P. elatior* (L.) hill raw materials. *International Journal of Environmental Analytical Chemistry*, *2017*, 2871579.

Barak, T. H., Kurt-Celep, I., Dilek-Tepe, H., Bardakcı, H., Akaydın, G., Yesilada, E., & Celep, E. (2023). In vitro assessment of dermatological activity potential of *Achillea clypeolata* Sm. in H_2O_2-treated human dermal fibroblasts. *South African Journal of Botany*, *160*, 1–8.

Barak, T. H., Kurt Celep, I., Şentürk, T. B., Bardakci, H., & Celep, E. (2022). In vitro anti-aging potential evaluation of *Maclura pomifera* (Rafin.) Schneider 80% methanol extract with quantitative HPTLC analysis. *Turkish Journal of Pharmaceutical Sciences*, *19*(4), 400–407.

Basavarajappa, G. M., Rehman, A., Shiroorkar, P. N., Sreeharsha, N., Anwer, Md. K., & Aloufi, B. (2023). Therapeutic effects of Crataegus monogyna inhibitors against breast cancer. *Frontiers in Pharmacology*, *14*, 1187079.

Bayer, I. S. (2020). Hyaluronic acid and controlled release: a review. *Molecules*, *25*(11), 2649.

Bhosale, P. B., Kim, H. H., Abusaliya, A., Vetrivel, P., Ha, S. E., Park, M. Y., Lee, Ho J., & Kim, G. S. (2022). Structural and functional properties of activator protein-1 in cancer and inflammation. *Evid Based Complement Alternat Med*, *2022*, 9797929.

Chaiyana, W., Chansakaow, S., Intasai, N., Kiattisin, K., Lee, K.-H., Lin, W.-C., Lue, S.-C., & Leelapornpisid, P. (2020). Chemical constituents, antioxidant, anti-MMPs, and anti-hyaluronidase activities of *Thunbergia laurifolia* Lindl. Leaf extracts for skin aging and skin damage prevention. *Molecules*, *25*(8), 1923.

Chen, C.-Y., Zhang, J. Q., Li, L., Guo, M. M., He, Y. F., Dong, Y. M., Meng, H., & Yi, F. (2022). Advanced glycation end products in the skin: molecular mechanisms, methods of measurement, and inhibitory pathways. *Frontiers in Medicine*, *9*, 00–00.

Colombo, P. S., Flamini, G., Rodondi, G., Giuliani, C., Santagostini, L., & Fico, G. (2017). Phytochemistry of European *Primula* species. *Phytochemistry*, *143*, 132–144.

Coran, S. A., & Mulas, S. (2012). Validated determination of primulasaponins in *Primula* root by a high-performance-thin-layer-chromatography densitometric approach. *Journal of Pharmaceutical and Biomedical Analysis*, *70*, 647–651.

Della Valle, A., Dimmito, M. P., Zengin, G., Pieretti, S., Mollica, A., Locatelli, M., Cichelli, A., Novellino, E., Ak, G., & Yerlikaya, S. (2020). Exploring the nutraceutical potential of dried pepper *Capsicum annuum* L. on market from Altino in Abruzzo Region. *Antioxidants (Basel)*, *9*(5), 00–00.

Demasi, S., Caser, M., & Scariot, V. (2023). Hot and cold drying of edible flowers affect metabolite patterns of extracts and decoctions. *Folia Horticulturae*, *35*(1), 193–207.

Demir, S., Turan, I., & Aliyazicioğlu, Y. (2019). Antioxidant properties of *Primula vulgaris* flower extract and its cytotoxic effect on human cancer cell lines. *Kahramanmaraş Sütçü İmam Üniversitesi Tarım ve Doğa Dergisi*, *22*(1), 78–84.

Demir, S., Turan, I., & Aliyazicioğlu, Y. (2019). Antioxidant properties of *Primula vulgaris* flower extract and its cytotoxic effect on human cancer cell lines. *Kahramanmaraş Sütçü İmam Üniversitesi Tarım ve Doğa Dergisi*, *22*(1), 78–84.

Dumanović, J., Nepovimova, E., Natić, M., Kuča, K., & Jaćević, V. (2021). The significance of reactive oxygen species and antioxidant defense system in plants: A concise overview. *Frontiers in Plant Science*, *11*, 00–00.

Elekofehinti, O. O., Iwaloye, O., Olawale, F., & Ariyo, E. O. (2021). Saponins in cancer treatment: current progress and future prospects. *Pathophysiology*, *28*(2), 250–272.

Ersoy, E., Eroglu Ozkan, E., Boga, M., Yilmaz, M. A., & Mat, A. (2019). Anti-aging potential and anti-tyrosinase activity of three Hypericum species with focus on phytochemical composition by LC–MS/MS. *Industrial Crops and Products*, *141*, 111735.

Fang, J., Ouyang, M., Qu, Y., Wang, M., Huang, X., Lan, J., Lai, W., & Xu, Q. (2022). Advanced glycation end products promote melanogenesis by activating NLRP3 inflammasome in human dermal fibroblasts. *Journal of Investigative Dermatology*, *142*(10), 2591–2602.e8.

Fock, E. M., & Parnova, R. G. (2021). Protective effect of mitochondria-targeted antioxidants against inflammatory response to lipopolysaccharide challenge: A review. *Pharmaceutics*, *13*(2), 144.

Gevrenova, R., Zheleva-Dimitrova, D., Balabanova, V., Voynikov, Y., Sinan, K. I., Mahomoodally, M. F., & Zengin, G. (2020). Integrated phytochemistry, bio-functional potential and multivariate analysis of *Tanacetum macrophyllum* (Waldst. & Kit.) Sch. Biand Telekia speciosa (Schreb.) Baumg. (Asteraceae). *Industrial Crops and Products*, *155*, 112817.

Gevrenova, R., Zengin, G., Sinan, K. I., Zheleva-Dimitrova, D., Balabanova, V., Kolmayer, M., Voynikov, Y., & Joubert, O. (2022). An in-depth study of metabolite profile and biological potential of *Tanacetum balsamita* L. (Costmary). *Plants*, *12*(1), 22.

Gkogkolou, P., & Böhm, M. (2012). Advanced glycation end products. *Dermato-Endocrinology*, *4*(3), 259–270.

Gonfa, Y. H., Tessema, F. B., Bachheti, A., Rai, N., Tadesse, M. G., Nasser Singab, A., Chaubey, K. K., & Bachheti, R. K. (2023). Anti-inflammatory activity of phytochemicals from medicinal plants and their nanoparticles: A review. *Current Research in Biotechnology*, *6*, 100152.

Grochowski, D. M., Uysal, S., Aktumsek, A., Granica, S., Zengin, G., Ceylan, R., Locatelli, M., & Tomczyk, M. (2017). In vitro enzyme inhibitory properties, antioxidant activities, and phytochemical profile of Potentilla thuringiaca. *Phytochemistry Letters*, *20*, 365–372.

Guarneri, F., Custurone, P., Papaianni, V., & Gangemi, S. (2021). Involvement of RAGE and oxidative stress in inflammatory and infectious skin diseases. *Antioxidants*, *10*(1), 82.

Hsu, H.-Y., & Wen, M.-H. (2002). Lipopolysaccharide-mediated reactive oxygen species and signal transduction in the regulation of interleukin-1 gene expression. *Journal of Biological Chemistry*, *277*(25), 22131–22139.

Huang, J., Wang, X., Zheng, J., Jia, Q., Wang, X., Xie, Z., & Ma, H. (2023). Mechanisms underlying the therapeutic effects of isoflavones isolated from chickpea sprouts in treating osteoporosis based on network pharmacology. *Biochemical and Biophysical Research Communications*, *671*, 26–37.

Iqbal, J., Abbasi, B. A., Ahmad, R., Mahmood, T., Kanwal, S., Ali, B., Khalil, A. T., Shah, S. A., Alam, M. M., & Badshah, H. (2018). Ursolic acid a promising candidate in the therapeutics of breast cancer: Current status and future implications. *Biomedicine & Pharmacotherapy*, *108*, 752–756.

Iqbal, J., Abbasi, B. A., Batool, R., Mahmood, T., Ali, B., Khalil, A. T., Kanwal, S., Shah, S. A., & Ahmad, R. (2018). Potential phytocompounds for developing breast cancer therapeutics: Nature's healing touch. *European Journal of Pharmacology*, *827*, 125–148.

Jacquemyn, H., Endels, P., Brys, R., Hermy, M., & Woodell, S. R. J. (2009). Biological flora of the British isles: *Primula vulgaris* Huds. (*P. acaulis* (L.) Hill). *Journal of Ecology*, *97*(4), 812–833.

Jäger, A. K., Gauguin, B., Adsersen, A., & Gudiksen, L. (2006). Screening of plants used in Danish folk medicine to treat epilepsy and convulsions. *Journal of Ethnopharmacology*, *105*(1-2), 294–300.

Jiratchayamaethasakul, C., Ding, Y., Hwang, O., Im, S.-T., Jang, Y., Myung, S.-W., Lee, J. M., Kim, H.-S., Ko, S.-C., & Lee, S.-H. (2020). In vitro screening of elastase, collagenase, hyaluronidase, and tyrosinase inhibitory and antioxidant activities of 22 halophyte plant extracts for novel cosmeceuticals. *Fisheries and Aquatic Sciences*, *23*(1), 6.

Jo, S., Kim, T., Iyer, V. G., & Im, W. (2008). CHARMM-GUI: a web-based graphical user interface for CHARMM. *Journal of computational chemistry*, *29*(11), 1859–1865.

Jomova, K., Alomar, S. Y., Alwasel, S. H., Nepovimova, E., Kuca, K., & Valko, M. (2024). Several lines of antioxidant defense against oxidative stress: Antioxidant enzymes, nanomaterials with multiple enzyme-mimicking activities, and low-molecular-weight antioxidants. *Archives of Toxicology*, *98*(5), 1323–1367.

Jurca, T., Marian, E., Vicas, L., Oana, N., & Pallag, A. (2015). Bioactive compounds and antioxidant capacity of *Primula veris* L. *flower extracts*, *00*, 00–00.

Kahraman, C., Sari, S., Küpeli Akkol, E., & Tatli Cankaya, I. (2022). Bioactive saponins of *Primula vulgaris* huds. Promote wound healing through inhibition of collagenase and elastase enzymes: In vivo, in vitro and in silico evaluations. *Chemistry & Biodiversity*, *19*(12), E202200582.

Kocyigit, A., Guler, E. M., & Dikilitas, M. (2018). *Role of antioxidant phytochemicals in prevention, formation and treatment of cancer*. Reactive oxygen species (ROS) in living cells (pp. 21–45). London: InterchOpen.

Kurt-Celep, I., Zengin, G., Celep, E., Dall'acqua, S., Sut, S., Ferrase, I., Ak, G., Uba, A. I., Polat, R., Canlı, D., Darendelioglu, E., Aumeeruddy, M. Z., Shariati, M. A., & Mahomoodally, M. F. (2023). A multifunctional key to open a new window on the path to natural resources-lessons from a study on chemical composition and biological capability of *Paeonia mascula* L. from Turkey. *Food Bioscience*, *51*, 102194.

Kurt-Celep, I., Zheleva-Dimitrova, D., Gevrenova, R., Uba, A. I., Zengin, G., Yıldıztugay, E., Picot-Allain, C. M. N., Lorenzo, J. M., Mahomoodally, M. F., & Montesano, D. (2022). An in-depth study on the metabolite profile and biological properties of *Primula auriculata* extracts: A fascinating sparkle on the way from nature to functional applications. *Antioxidants*, *11*(7), 1377.

Kurt-Celep, I., Zheleva-Dimitrova, D., Sinan, K. I., Uba, A. I., Nilofar, Mahomoodally, M. F., Aumeeruddy, M. Z., Cakilcioglu, U., Dall'acqua, S., & Zengin, G. (2024). Uncovering chemical profiles, biological potentials, and protection effect against ECM destruction in H2O2-treated HDF cells of the extracts of *Stachys tundjeliensis*. *Archiv der Pharmazie*, *357*(2), 2300528.

Kurt-Celep, I., Zengin, G., Sinan, K. I., Ak, G., Elbasan, F., Yıldıztugay, E., Maggi, F., Caprioli, G., Angeloni, S., Sharmeen, J. B., & Mahomoodally, M. F. (2021). Comprehensive evaluation of two Astragalus species (*A. campylosema* and *A. hirsutus*) based on biological, toxicological properties and chemical profiling. *Food and Chemical Toxicology*, *154*, 112330.

Kurt-Celep, I., Nihan Kilinc, A., Griffin, M., & Telci, D. (2022). Nitrosylation of tissue transglutaminase enhances fibroblast migration and regulates MMP activation. *Matrix Biology*, *105*, 1–16.

Kurt-Celep, I., Zengin, G., Uba, A. I., Caprioli, G., Mustafa, A. M., Angeloni, S., Cakilcioglu, U., Guler, O., Kaplan, A., Sharmeen, J., & Mahomoodally, M. F. (2023). Unraveling the chemical profile, antioxidant, enzyme inhibitory, cytotoxic potential of different extracts from Astragalus caraganae. *Archiv der Pharmazie*, *356*(9), 2300263.

Loo, Y. C., Hu, H.-C., Yu, S.-Y., Tsai, Yi-H., Korinek, M., Wu, Y.-C., Chang, F.-R., & Chen, Y.-J. (2023). Development on potential skin anti-aging agents of Cosmos caudatus Kunth via inhibition of collagenase, MMP-1 and MMP-3 activities. *Phytomedicine*, *110*, 154643.

Länger, R. R. (2012). *Assessment report on* Primula veris *L. and/or* Primula elatior *(L.) Hill*, *flos*. European Medicines Agency.

Lu, P., Takai, K., Weaver, V. M., & Werb, Z. (2011). Extracellular matrix degradation and remodeling in development and disease. *Cold Spring Harb Perspect Biol*, *3*(12), 00.

Lupitu, A., Tomescu, D., Mot, C. A., Moisa, C., Copolovici, D. M., & Copolovici, L. (2018). Variation in phenolic content and antioxidant activity of different plant parts of *Primula veris*. Scientific Bulletin. Series F. Biotechnologies, *8*, 50–53.

Mahran, E., El Gamal, I., Keusgen, M., & Morlock, G. E. (2019). Effect-directed analysis by high-performance thin-layer chromatography for bioactive metabolites tracking in *Primula veris* flower and *Primula boveana* leaf extracts. *Journal of Chromatography A*, *1605*, 460371.

Maier, J. A., Martinez, C., Kasavajhala, K., Wickstrom, L., Hauser, K. E., & Simmerling, C. (2015). ff14SB: Improving the accuracy of protein side chain and backbone parameters from ff99SB. *Journal of Chemical Theory and Computation*, *11*(8), 3696–3713.

Mcgleenon, Dynan, & Passmore, (1999). Acetylcholinesterase inhibitors in Alzheimer's disease. *British journal of clinical pharmacology*, *48*(4), 471.

Meertens, J. H., Nienhuis, H. L., Lefrandt, J. D., Schalkwijk, C. G., Nyyssönen, K., Ligtenberg, J. J. M., Smit, A. J., Zijlstra, J. G., & Mulder, D. J. (2016). The course of skin and serum biomarkers of advanced glycation endproducts and its association with oxidative stress, inflammation, disease severity, and mortality during ICU admission in critically ill patients: results from a prospective pilot study. *PLOS ONE*, *11*(8), E0160893.

Meos, A., Zaharova, I., Kask, M., & Raal, A. (2017). Content of ascorbic acid in common cowslip (*Primula veris* L.) compared to common foodplants and orange juices. *Acta Biologica Cracoviensia s. Botanica*, *59/1*, 113–120.

Michel, P., Granica, S., Rosińska, K., Glige, M., Rojek, J., Poraj, Ł., & Olszewska, M. A. (2022). The effect of standardised leaf extracts of *Gaultheria procumbens* on multiple oxidants, inflammation-related enzymes, and pro-oxidant and pro-inflammatory functions of human neutrophils. *Molecules*, *27*(10), 3357.

Mohammed, A. B. A., Yagi, S., Tzanova, T., Schohn, H., Abdelgadir, H., Stefanucci, A., Mollica, A., Mahomoodally, M. F., Adlan, T. A., & Zengin, G. (2020). Chemical profile, antiproliferative, antioxidant and enzyme inhibition activities of *Ocimum basilicum* L. and *Pulicaria undulata* (L.) C.A. Mey. grown in Sudan. *South African Journal of Botany*, *132*, 403–409.

Mohamed, A. G., Fouad, M. A., Ibrahim, S. R. M., & Elkhayat, E. (2014). Antioxidant and anti-inflamatory activities of phenolic constituents from *Primula elatior* L. aerial part. *International Journal of Pharmacognosy and Phytochemical Research*, *6*, 74–78.

Mostafa, F. A., Gamal, M. A., Sabrin, I. R., & Ehab, E. S. (2014). Antioxidant and anti-inflamatory activities of phenolic constituents from Primula elatior L. aerial part. *Int International Journal of Pharmacognosy and Phytochemical Research*, *6*, 74–78.

Mosxou, D., & Letsiou, S. (2021). Exploring the protective effects of phaeodactylum tricornutum extract on LPS-treated fibroblasts. *Cosmetics*, *8*(3), 76.

Naidu, M. U. R., Ramana, G. V., Rani, P. U., Mohan, L. K., Suman, A., & Roy, P. (2004). Chemotherapy-induced and/or radiation therapy-induced oral mucositis-complicating the treatment of cancer. *Neoplasia*, *6*(5), 423–431.

Nelson, V. K., Sahoo, N. K., Sahu, M., Sudhan, H. H., Pullaiah, C. P., & Muralikrishna, K. S. (2020). In vitro anticancer activity of *Eclipta alba* whole plant extract on colon cancer cell HCT-116. *BMC Complementary Medicine and Therapies*, *20*, 1–8.

Nennig, S. E., & Schank, J. R. (2017). The role of NFkB in drug addiction: beyond inflammation. *Alcohol and Alcoholism*, *52*(2), 172–179.

Nguyen, Q. T. N., Fang, M., Zhang, M., Do, N. Q., Kim, M., Zheng, S. D., Hwang, E., & Yi, T. H. (2021). Crataegus laevigata suppresses LPS-induced oxidative stress during inflammatory response in human keratinocytes by regulating the MAPKs/AP-1, NFκB, and NFAT signaling pathways. *Molecules*, *26*(4), 869.

Nilofar, N., Zengin, G., Acar, M., Bouyayha, A., Youssra, A., Eldahshan, O., Fayez, S., & Fahmy, N. (2024). Assessing the chemical composition, antioxidant and enzyme inhibitory effects of *Pentapleura subulifera* and *Cyclotrichium glabrescens* extracts. *Chemistry & Biodiversity*, *21*(2), E202301651.

Ozkan, M., Aliyazicioğlu, R., Demir, S., Misir, S., Turan, I., Yildirmiş, S., & Aliyazicioğlu, Y. (2017). Phenolic characterisation and antioxidant activity of *Primula vulgaris* and its antigenotoxic effect on fibroblast cells. *Jundishapur Journal of Natural Pharmaceutical Products*, *12*(1), 00–00.

Ozkan, M., Aliyazicioglu, R., Demir, S., Misir, S., Turan, I., Yildirmis, S., & Aliyazicioglu, Y. (2017). Phenolic characterisation and antioxidant activity of *Primula vulgaris* and its antigenotoxic effect on fibroblast cells. *Jundishapur Journal of Natural Pharmaceutical Products*, *12*(1), e40073.

Park, J., Min, Ju-S., Kim, B., Chae, U.-B., Yun, J. W., Choi, M.-S., Kong, I.-K., Chang, K.-T., & Lee, D.-S. (2015). Mitochondrial ROS govern the LPS-induced pro-inflammatory response in microglia cells by regulating MAPK and NF-κB pathways. *Neuroscience Letters*, *584*, 191–196.

Pascale, R., Acquavia, M. A., Cataldi, T. R. I., Onzo, A., Coviello, D., Bufo, S. A., Scrano, L., Ciriello, R., Guerrieri, A., & Bianco, G. (2020). Profiling of quercetin glycosides and acyl glycosides in sun-dried peperoni di Senise peppers (*Capsicum annuum* L.) by a combination of LC-ESI (-)-MS/MS and polarity prediction in reversed-phase separations. *Analytical and Bioanalytical Chemistry*, *412*, 3005–3015.

Pucci, C., Martinelli, C., & Ciofani, G. (2019). Innovative approaches for cancer treatment: Current perspectives and new challenges. *ecancermedicalscience*, *13*, 00–00.

Richards, J. (2014). *Primula*. Batsford Books.

Ronsisvalle, S., Panarello, F., Longhitano, G., Siciliano, E. A., Montenegro, L., & Panico, A. (2020). Natural flavones and flavonols: Relationships among antioxidant activity, glycation, and metalloproteinase inhibition. *Cosmetics*, *7*(3), 71.

Ruddon, R. W. (2007). *Cancer biology*. Oxford University Press.

Schmidt-Lebuhn, A. N., De Vos, J. M., Keller, B., & Conti, E. (2012). Phylogenetic analysis of Primula section Primula reveals rampant non-monophyly among morphologically distinct species. *Molecular Phylogenetics and Evolution*, *65*(1), 23–34.

Serasanambati, M., & Chilakapati, S. R. (2016). Function of nuclear factor Kappa B (NF-kB) in human diseases—A review. *South Indian Journal of Biological Sciences*, *2*, 368–387.

Shen, Y., Song, X., Li, L., Sun, J., Jaiswal, Y., Huang, J., Liu, C., Yang, W., Williams, L., Zhang, H., & Guan, Y. (2019). Protective effects of p-coumaric acid against oxidant and hyperlipidemia-an in vitro and in vivo evaluation. *Biomedicine & Pharmacotherapy*, *111*, 579–587.

Shi, J., Shi, S., Xie, W., Zhao, M., Li, Y., Zhang, J., Li, N., Bai, X., Cai, W., Hu, X., Hu, D., Han, J., & Guan, H. (2021). IL-10 alleviates lipopolysaccharide-induced skin scarring via IL-10R/STAT3 axis regulating TLR4/NF-κB pathway in dermal fibroblasts. *Journal of Cellular and Molecular Medicine*, *25*(3), 1554–1567.

Siegel, R. L., Miller, K. D., Goding Sauer, A., Fedewa, S. A., Butterly, L. F., Anderson, J. C., Cercek, A., Smith, R. A., & Jemal, A. (2020). Colorectal cancer statistics, 2020. *CA: A Cancer Journal for Clinicians*, *70*(3), 145–164.

Singh, S., Sharma, B., Kanwar, S. S., & Kumar, A. (2016). Lead phytochemicals for anticancer drug development. *Frontiers in Plant Science*, *7*, 224341.

Singh, S., & Singh, T. G. (2020). Role of nuclear factor Kappa B (NF-κB) signalling in neurodegenerative diseases: An mechanistic approach. *Curr Neuropharmacol*, *18*(10), 918–935.

Slinkard, K., & Singleton, V. L. (1977). Total phenol analysis: Automation and comparison with manual methods. *American journal of enology and viticulture*, *28*(1), 49–55.

Stefanis, I., Chatzopoulou, P., Krigas, N., & Karioti, A. (2023). Exploring the chemical content of *Primula veris* L. subsp. veris wild-growing populations along a climate gradient: An HPLC-PDA-MS quality assessment of flowers, leaves and roots for sustainable exploitation. *Horticulturae*, *9*(10), 1120.

Subedi, L., Lee, J., Yumnam, S., Ji, E., & Kim, S. (2019). Anti-inflammatory effect of sulforaphane on LPS-activated microglia potentially through JNK/AP-1/NF-κB inhibition and Nrf2/HO-1 activation. *Cells*, *8*(2), 194.

Suhail, M., Alzahrani, W. M., Shakil, S., Tarique, M., Tabrez, S., Zughaibi, T. A., & Rehan, M. (2023). Analysis of some flavonoids for inhibitory mechanism against cancer target phosphatidylinositol 3-kinase (PI3K) using computational tool. *Frontiers in Pharmacology*, *14*, 1236173.

Sul, O.-J., & Ra, S. W. (2021). Quercetin prevents LPS-induced oxidative stress and inflammation by modulating NOX2/ROS/NF-kB in lung epithelial cells. *Molecules*, *26*(22), 6949.

Sun, B. (2021). The mechanics of fibrillar collagen extracellular matrix. *Cell Reports Physical Science*, *2*(8), 100515.

Talreja, S., & Tiwari, D. (2023). A complete overview on *Primula vulgaris*. *International Journal of Life Science and Pharma Research*, *13*, 277–286.

Tarapatskyy, M., Gumienna, A., Sowa, P., Kapusta, I., & Puchalski, C. (2021). Bioactive phenolic compounds from *Primula veris* L.: Influence of the extraction conditions and purification. *Molecules*, *26*(4), 997.

Teng, B., Lu, Y., Wang, Z., Tao, X., & Wei, D. (2006). In vitro anti-tumor activity of isorhamnetin isolated from *Hippophae rhamnoides* L. against BEL-7402 cells. *Pharmacol Res*, *54*(3), 186–194.

Trott, O., & Olson, A. J. (2010). AutoDock Vina: Improving the speed and accuracy of docking with a new scoring function, efficient optimization, and multithreading. *Journal of Computational Chemistry*, *31*(2), 455–461.

Turan, I., Canbolat, D., Demir, S., Kerimoglu, G., Colak, F., Turkmen Alemdar, N., Mentese, A., & Aliyazicioglu, Y. (2023). The ameliorative effect of *Primula vulgaris* on cisplatin-induced nephrotoxicity in rats and quantification of its phenolic components using LC-ESI-MS/MS. *Saudi Pharmaceutical Journal*, *31*(9), 101730.

Wisetkomolmat, J., Suksathan, R., Puangpradab, R., Kunasakdakul, K., Jantanasakulwong, K., Rachtanapun, P., & Sommano, S. R. (2020). Natural surfactant saponin from tissue of *Litsea glutinosa* and its alternative sustainable production. *Plants*, *9*(11), 1521.

Wu, Y., & Zhou, B. P. (2010). TNF-α/NF-κB/Snail pathway in cancer cell migration and invasion. *British Journal of Cancer*, *102*(4), 639–644.

Yaylı, N., Tosun, G., Yaylı, B., Gündoğanc, Z., Coşkunçelebic, K., & Karaoğlu, Ş. A. (2016). Altitude variation in the composition of essential oils, fatty acid methyl esters, and antimicrobial activities of two subspecies of *Primula vulgaris* grown in Turkey. *Natural Product Communications*, *11*(10), 1934578×1601101020.

Yerlikaya, S., Zengin, G., Mollica, A., Baloglu, M. C., Celik Altunoglu, Y., & Aktumsek, A. (2017). A multidirectional perspective for novel functional products: In vitro pharmacological activities and in silico studies on *Ononis natrix* subsp. hispanica. *Frontiers in Pharmacology*, *8*, 600.

Yuandani, Jantan, I., Salim, E., Septama, A. W., Rullah, K., Nainu, F., Fasihi Mohd Aluwi, M. F., Emran, T. B., Roney, M., Khairunnisa, N. A., Nasution, H. R., Fadhil As'ad, M., Shamsudin, N. F., Abdullah, M. A., Marwa Rani,

H. L., Al Chaira, D. M., & Aulia, N. (2024). Mechanistic insights into anti-inflammatory and immunosuppressive effects of plant secondary metabolites and their therapeutic potential for rheumatoid arthritis. *Phytotherapy Research*, *38*(6), 2931–2961.

Zengin, G., Senkardes, I., Mollica, A., Picot-Allain, C. M. N., Bulut, G., Dogan, A., & Mahomoodally, M. F. (2018). New insights into the in vitro biological effects, in silico docking and chemical profile of clary sage—*Salvia sclarea* L. *Computational Biology and Chemistry*, *75*, 111–119.

Zengin, G., Ferrante, C., Senkardes, I., Gevrenova, R., Zheleva-Dimitrova, D., Menghini, L., Orlando, G., Recinella, L., Chiavaroli, A., Leone, S., Brunetti, L., Picot-Allain, C. M. N., Rengasamy, K. R. R., & Mahomoodally, M. F. (2019). Multidirectional biological investigation and phytochemical profile of *Rubus sanctus* and *Rubus ibericus*. *Food and Chemical Toxicology*, *127*, 237–250.

Zheleva-Dimitrova, D., Simeonova, R., Kondeva-Burdina, M., Savov, Y., Balabanova, V., Zengin, G., Petrova, A., & Gevrenova, R. (2023). Antioxidant and hepatoprotective potential of *Echinops ritro* L. extracts on induced oxidative stress in vitro/in vivo. *International Journal of Molecular Sciences*, *24*(12), 9999.

SUPPORTING INFORMATION

Additional supporting information can be found online in the Supporting Information section at the end of this article.

How to cite this article: Kurt-Celep, I., Nilofar, Cetiz, M. V., Zheleva-Dimitrova, D., Gevrenova, R., Celep, E., Sinan, K. I., Yildiztugay, E., Ferrante, C., & Zengin, G. (2024). From small-scale studies to an encompassing view: Inhibiting inflammation and clinically relevant enzymes with various extracts of *Primula vulgaris* using in vitro and in silico techniques. *Food Frontiers*, 1–31. https://doi.org/10.1002/fft2.473